Efficient Energy Control Strategies for a Standalone Renewable/Fuel Cell Hybrid Power Source

Nicu Bizon[1)2)], Mihai Oproescu[1)], Mircea Raceanu[3)2)]
[1)]University of Pitesti, 1 Targu din Vale, Arges, 110040 Pitesti, Romania
[2)]University Politehnica of Bucharest, 313 Splaiul Independentei, 060042 Bucharest, Romania
[3)] National Center for Hydrogen and Fuel Cell National Research and Development Institute for Cryogenics and Isotopic Technologies, ICIT Rm. Valcea, Romania,
Tel +40 348 453 201, Fax +40 348 453 200; nicubizon@yahoo.com, nicu.bizon@upit.ro

Abstract: In this paper, four energy control strategies are proposed and analyzed for the Standalone Renewable / Fuel Cell Hybrid Power Source (RES/FC HPS). The concept of the Load Following (LF) and Maximum Efficiency Point Tracking (MEPT) is used to control the fueling rates. A standalone RES/FC HPS uses at least one Renewable Energy Sources (RES) and a Polymer Electrolyte Membrane (PEM) Fuel Cell (FC) as backup source. Photovoltaic (PV) array and wind turbines (WT) farm are used as RES and the surplus of energy during light load stages is stored in hydrogen tank via water electrolysis to fuel the PEMFC. Small-scale RESs and commercially available PEMFCs are interfaced to the common DC bus via power converters and then to the single-phase distribution grid through a voltage source inverter. RES/FC HPS seem to be an efficient alternative for supplying smart houses and isolated sites. This paper proposes a new supervision strategy of the Energy Management Unit (EMU) based on the LF control approach that assures a charge-sustaining (CS) mode for the Energy Storage System (ESS). So, the capacity of the batteries stack can be reduced at minimum if it is directly connected to the DC bus. The ultracapacitors stack compensates dynamically the power flow balance on the DC bus, regulating the DC voltage via a bidirectional buck-boost power converter. Thus, a semi-active hybrid topology is adopted for the ESS having the batteries stack. The MEPT loops ensure an optimized energy management of the RES/FC HPS. The LF strategy designed based on the power flow balance guarantees the load demand through the efficient management of the power flow from RES, FC and ESS, adapting FC energy production to load profile. The FC energy production is controlled via the fueling rates (one is controlled in the LF loop and the other is controlled in the MEPT loop) to maximize the energy consumption indicator: the ratio of the produced energy and the fuel consumed by the FC system during a load cycle. Thus, this paper evaluates the control performances of the four control topologies to fuel the FC stack during an variable RES and load profile. The MATLAB-Simulink® software package is used to model the RES/FC HPS and develop the four EMU strategies. Simulation results shown comparatively the performance of the EMU strategies proposed under different scenarios of RES power generation and load demand.

Keywords: Fuel Cell Hybrid Power Source; Renewable energy; Energy efficiency; Maximum Efficiency Point Tracking; Energy management strategy.

List of abbreviations:
Air Flow rate – AirFr
Average – AV
Band-Pass Filter - BPF
Charge-Sustaining – CS
Energy Management Unit – EMU
Extremum Seeking – ES
Equivalent Series Resistors – ESR
Energy Storage System – ESS
Equivalent Parallel Resistors – EPR
Fuel Cell - FC
Fuel Flow rate – FuelFr
High-Pass Filter – HPF
Hybrid Power Source - HPS
Maximum Efficiency Point Tracking – MEPT
Maximum Power Point Tracking – MPPT

PEM Fuel Cell - PEMFC
Perturb and Observe - P&O
Photovoltaic - PV
Polymer Electrolyte Membrane – PEM
Renewable Energy Source – RES
Single-Input Double-Outputs – SIDO
Single-Input Single-Output - SISO
State-Of-Charge – SOC
Static Feed-Forward – sFF
Wind Turbines – WT

1. Introduction

The environment could be protected from further deterioration if the RESs will be used more intensive in energy production. Furthermore, the solar and wind energy are free and clean, but available at variable levels related to the local environment parameters (insolation, wind speed and temperature). Besides, the long lifetime and low maintenance requirements recommend these types of RESs [1]. The combinations of PV and WT systems with ESS for the surplus of RES energy or lack of power under load peaks have a widespread use [2–10]. The main feature of RES HPS is to combine more than one RES technology, optimizing their power flows in order to obtain efficiencies higher than that could be obtained from a single RES [2]. Thus, the RES HPS can address limitations in terms of RES power variability, variable load demand, efficiency, reliability, emissions and implementing costs [3,4]. Because the electricity consumption in the residential sector represents more than 30% of the overall energy consumption [2], the importance of optimization strategies of the energy usage in a smart house is obvious [5,6].

Besides RESs, the RES HPS can contain one conventional energy sources, such a diesel generator, which will operate as backup energy source in standalone or grid connected mode [7].

In last decade, the diesel generator is replaced by the FC systems [8,9] due to its disadvantages such as greenhouse emissions, high maintenance costs, and low scalability to meet changing in load demands [10].

Thus, the RES/FC HPS with hydrogen storage ensures eco-friendly operation, being scalable for small- and medium scale power applications [11, 12, 13]. Consequently, the hydrogen production via the eco-friendly process of water electrolysis is proposed as alternative to expensive and unsafe solution of hydrogen storage in tanks [12]

Anyway, some issues related to the FC use (such as fuel starvation phenomenon, safe operation, high cost of the membrane and catalyst, and so on) are still in researchers' attention [13]. However, the RES/FC HPS can provide multifold advantages based on EMU strategies proposed [14]. The LF control loop was proposed for a FC HPS (without support of the RESs) in [15], but this strategy could be also used in control of an active power filter for a solid oxide FC [16] or efficient operation of combined heat and power system [17]. The EMU strategy proposed here based on the LF and MEPT control loops set the fueling rates considering the average (AV) of the FC power requested on the DC bus and then generates the maximum net FC for these fueling rates. Thus, the efficiency of the whole HPS increase, the fuel consumption is minimized, and the ESS behavior and life-cycle are improved. The AV value of the FC net power and then the reference current are evaluated in the LF control block based on mean-value block, but other signal processing techniques could be used as well [3,8]. The reference current is used to set one of the fueling rates. The MEPT controller harvests the maximum available FC net power that can be generated by searching the MEP via the other fueling rate. The advantages of the four fueling topologies based on the LF and MEPT loops are shown in this paper.

Note that EMU meta-rules to ensure the energy dispatch between the DC bus and the electrolyzer or plug-in electrical vehicle during an energy surplus (RES power higher than load demand) is only mentioned here, being intensively studied in the literature [11-14,18]. Also, the optimization of the load demand through scheduling the non-priority loads is outside the scope of this paper. The LF control is proposed here to make face efficiently to all load profile if the energy sources and backup source are properly designed [7-12,19].

A PEMFC is used as backup source because of the advantages of this technology related to other FC technologies [13-15,20]. In addition, the hydrogen is abundant in the nature and can be obtained by reforming the natural gas, ethanol, methanol, biogas, and so on, or by water electrolyzing. Besides the eco-friendly

operation of the RES/FC HPS, the economic aspect makes the PEMFC a competitive technology in comparison to diesel generator, offering a reduced maintenance effort and cost [5-6,21].
So, integrating RES, FC and ESS into a RES/FC HPS via a multiport power converter (see Figure 1), the hybrid source will have the energy generation/storage support to make face to energy consumption and variability of the RES power that are not always synchronized with the load demand. Thus, EMU strategies are important in optimizing the energy management of the energy sources [1-4, 9, 11-15, 21]. The main goal of the EMU strategies must to ensure the load demand. Besides this, the other specific goals of the EMU strategies must be related to fuel consumption, energy efficiency of the energy sources that must to be also safe operated, life cycle of the HPS, and cost [11-15, 21-22].

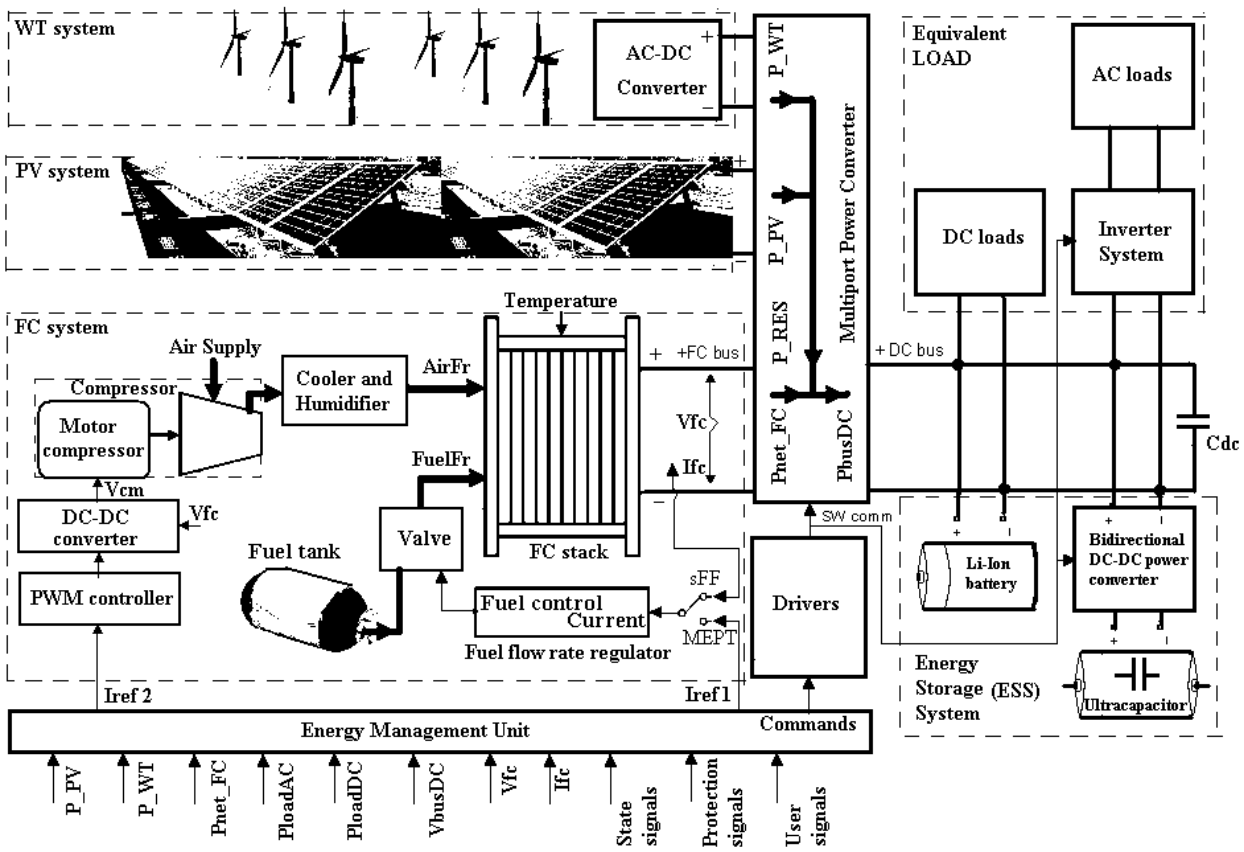

Figure 1. The standalone Renewable/Fuel Cell Hybrid Power Source system

Consequently, some variables of the HPS (named in Figure 1 as state signals; for example the state-of-charge (SOC) level of the ESS devices) and control variables (for example the DC bus voltage, FC current, load demand, and RES power level) must to be inputs of the EMU strategy. Besides these signals, the protection and user signals are used to safe operation of the HPS.
The studies above mentioned analyze the energy efficiency of the EMU strategies using dynamic models of the HPS based on short-term simulations with time scale of seconds [23] or minutes [24]. The voltage regulation on the DC bus of the PV/FC HPS is approached by classical linear or non-linear control algorithm (for example, based on the differential flatness principle [25]).
Different energy management strategies are proposed in the literature. For example, the fuzzy logic control was used in [26] to monitor the SOC of the ESS devices, improving the utilization costs and lifetime of the battery and hydrogen system as well. Also, the management of power flows between the FC and ESS in HPS grid connected is analyzed based on a fuzzy logic control [22,27] or ANFIS control [28]. The energy efficiency of a standalone RES/FC HPS based on EMU strategy to make face to RES power variations was investigated in [24,29].
In long-term analysis, the main goal of the EMU strategies is focused on meeting the load demand considering in the energy dispatch other specific goals such as the cost and the energy efficiency, and state signals such as

the SOC level of the ESS devices, etc. An adaptive predictive strategy for a RES/FC HPS to meet the above goals is analyzed with a time scale of hours in [30]. Three EMU strategies to meet the load demand and increase the energy efficiency based on long-term simulations throughout one year are proposed in [12,31]. Also, the expected lifetime of a standalone HPS was evaluated in [32].

The energy strategies mentioned above are mainly based on a monitoring of the power flows and states of the ESS devices to decide the energy dispatch between the FC and battery to the load [21,33]. In this paper, the battery operates in CS mode to minimize its size, the load demand being sustained based on the LF control proposed by the RESs and FC system. Also, it can be noted that the dynamics of the energy sources and especially of the power interfaces are frequently neglected [34]. The power converters are modeled in this paper using components from the SimPowerSystems library of the Matlab - Simulink® and not using an AV model that is recommended for a long-term analysis of the HPS behavior and performance. Thus, a short-term analysis will be performed here based on the sample frequency of the 10 kHz, which is more than enough to efficiently use the real profile of the RES power based on advanced Maximum Power Point Tracking (MPPT) control with high search speed and good tracking accuracy [23,35].

The MEPT technique based on the Extremum Seeking (ES) control scheme is used here to control one of the fueling rates [36], but note that any MEPT advanced technique could be used as well. The ES control is perturbed – based scheme, using dithers with different frequencies or orthogonal dithers to implement Single-Input Double-Outputs (SIDO) ES control scheme [37]. Note that only the performances of a PEMFC system are tested in [35-37], while here the performances of a whole RES/FC HPS are shown. Thus, besides the EMU that includes the LF and MEPT control schemes, the main components of the standalone RES/FC HPS includes a PV array, a set of wind generators, a FC system as backup source, a short–term ESS based on li-ion batteries and ultracapacitors, and a long-term ESS that consists of an electrolyzer and a hydrogen storage system with pressurized tanks (only this is shown in Figure 1), DC loads and AC load interfaced with inverters (named the equivalent load), and a multiport power converter or independent power interfaces for each energy sources and load.

Summarizing, the research directions in field of the RES/FC HPS that are approached in the studies mentioned above are the following [38]:

• The RES need advanced control techniques to harvest all power available, operating the RES close to MPP. This control is mandatory due to poor efficiency of solar PV, which is the main impediment in encouraging its use until the PV technology will be improved.

• The power losses in power interfaces have been substantially reduced using advanced topologies, switches and appropriate control scheme, eventually integrated in multiport power converter structure. In general, the energy efficiency of power converters used in HPS is higher than 95%.

• The hybrid batteries/ultracapacitors ESS is used in HPS to ensure the power flow balance on the DC bus, but their life-cycle need to be improved through innovative technologies, too. The CS mode proposed here for the ESS can improve the life-cycle of the batteries stack, besides other advantages such as reduced size and low costs of the ESS.

• The cost reduction could be an incentive for the producers of HPS to implement such systems that will ensure decreasing of the payback time for the capital invested.

• The hydrogen technology (to generate and store hydrogen) is still a costly and unsafe technology. So, alternative technologies based on fuel reformers are developed at low cost. Furthermore, the PEMFC system must be operated at the MEP to increase the energy efficiency of the entire RES/FC HPS, as it is proposed here.

• These standalone RES/FC HPSs based on EMU strategies must to predict the RES power available or be adaptable to RES power fluctuations to sustain any unpredictable load demand. The LF control proposed here could be o solution, because it is very simple to be implemented in the commercial RES/FC HPS, requesting only software upgrade and few circuits reconfiguration.

• The protection issue, especially for use of PEMFC system and batteries stack from the ESS, are identified and implemented in EMU of the commercial RES/FC HPS. The proposed protection measures are implemented in simulation diagram used here, but this issue was not extensively studied, being outside of the scope of this paper. For example, the recommended rate [39] to limit the FC current is used in all simulation shown in this paper.

In this paper, four new control topologies of the RES/FC HPS are introduced. The innovative idea is to use the LF control based on the MEPT control scheme to control efficiently both fueling rates in order to ensure the power flow balance on the DC bus. The main contributions of this paper are the following: (1) the LF control based on the MEPT control scheme is proposed to ensure the load demand and improve the energy efficiency of whole RES/FC HPS (2) the both fuel consumption and fuel efficiency are used as performances indicators; (3) a methodology to compare the four new control topologies of the RES/FC HPS is performed based on the performances indicators proposed; (4) the advantage of the LF control that operates the ESS in CS mode is shown under any load demand, with direct implications in the size and cost of the RES/FC HPS; (5) the advantage of the MEPT control that operates efficiently the FC stack is also shown considering the variability of RES and load power profiles, with direct implications in efficiency of the whole RES/FC HPS.
This paper is organized as follows. Section 2 presents briefly the issue related to unit sizing and optimization of the FC/RES HPS. The structure and control loops of the proposed RES/FC HPS unit are also explained here. The four EMU strategies to control the fueling rates are explained in Section 3 based on the AV power flow balance. The models of all units used in simulation of the RES/FC HPS are briefly shown in Section 4. The implementation of the LF and MEPT control loops are detailed in Section 5. The results obtained by comparing the proposed EMU strategies under constant load, random pulsed load, and variable load under different RES power profiles are shown and discussed in Section 6. Section 7 concludes the paper.

2. Standalone Renewable/Fuel Cell Hybrid Power Source

As it is known, the RESs have different operating characteristics, but in general these have a global MPP that must be tracked under different environment conditions. Also, the operating characteristic of the PEMFC system has a maximum (for example, the FC net power related to FC current). Thus, the usual method to integrate RES and FC into a RES/FC HPS is based on power interfaces controlled to track the MPP and MEP of the input energy source. Besides this general used connection of the energy sources to the DC bus [40], which define the DC bus configuration, there are other two possible configurations to integrate different RESs, FC and ESS into a RES/FC HPS: AC coupled configuration and Hybrid coupled configuration [27,41, 42]. In this paper, the DC coupled configuration and equivalent DC load concept is used to test the control performances under different RES and load power profiles.

2.1. Unit sizing and optimization

As it was mentioned on Introduction, the RESs have a random behavior. Thus, it is difficult to be predicted the available RES power flow in order to size the FC stack and ESS to make face to any load demand. In sunny and windy days the ESS is charged up to higher charge limit (set for the SOC) and electrolyzer refills the hydrogen tanks that are underutilized. Instead of this favorable case, the RES power flow is low during the cloudy days with moderate wind. Consequently, the ESS is discharged under the lower discharge limit, the electrolyzer is stopped, and the hydrogen tank may be empty, if this situation continues on a long period of time, which is difficult to be predicted under the current climate change. So, the size of the FC and batteries stack, the electrolyzer and hydrogen storage tanks must to be designed carefully considering the load demand and RES power flow available in all extreme weather conditions. Furthermore, the load demand of a smart home has also a random power profile. Thus, the unit sizing and optimization of standalone RES/FC HPS is not a trivial design problem, requiring an algorithm to size the HPS components by minimizing the system cost while maintaining system reliability [9-10]. It is obvious that the design objectives such as acceptable cost and reliability level are conflicting with one another [12,31]. For example, over sizing the HPS components will increase the HPS cost while under sizing can lead in lack of power to continuously sustain the load demand. So, the algorithms to size the HPS components must ensure a reasonable tradeoff between the design objectives, optimizing the HPS energy sources to achieve the target levels of cost and reliability. The HPS reliability is determined by estimating the loss of load probability, which is the ratio between estimated power deficit and the load demand during a load cycle, or appropriate other reliability indicators such loss of power probability, loss of power supply probability, and load coverage rate [42]. Besides the HPS cost and reliability, the sizing algorithms optimize the HPS components or other HPS parameters, such as investment cost, output energy cost, fuel consumption or appropriate other parameters such as net present cost, levelized cost of energy and fuel efficiency [43].

The algorithms to size the HPS components obviously depend on the availability of the weather data on short or long term, so two class are defined in the literature: conventional sizing algorithms based on weather data and expert algorithms if the weather data is not available or available only on short term, such is the case of remote isolated sites [19,41,42]. In first case, the concept of energy balance is a simple algorithm of sizing the HPS components [43]. In last case, the algorithms based on artificial intelligence are usually used [44, 45].
The rated power of the FC stack is set here to be higher than the maximum load demand because the sizing objective is outside the scope of this paper.

2.2. The structure of the proposed unit

The HPS unit structure based on RES and FC system that has a new fueling control strategy based on LF and ES control loops is proposed here (Figure 1). It is known that the FC stack needs an ESS under dynamic loads to improve the HPSs system performance under random load demand and random RES power profile [46]. The ESS topology used here is of semi-active type: batteries stack direct connected to the DC bus and ultracapacitors stack via a bidirectional power converter [47]. This hybrid ESS topology is usually used due their advantages: the SOC variation of the ultracapacitors stack in large range ensures the dynamically compensation of the power flow balance at reduced cost. Thus, the proposed HPS that is shown in Figure 1 is composed of energy sources (FC, WT, and PV systems), ESS (batteries and ultracapacitors stacks), equivalent load (AC and DC loads), multiport power converter, and EMU (containing the ES and LF controllers).
The fuel is classically or efficiently controlled based on static feed-forward (sFF) control or ES control scheme, which means the use of the FC current (I_{FC}) or the reference current 1 (I_{ref1}) for the fuel regulator to control the fuel flow rate (FuelFr). The second ES controller generates the reference current (I_{ref}) to control the FC power in the LF control loop (see Figure 2). The LF controller generates the reference current 2 (I_{ref2}) to control the air flow rate (AirFr) (Figure 1). Note that both ES controllers have as input the same signal, the FC net power (P_{FCnet}), as it shown in Figure 2. In fact, the unit structure shown in Figure 1 is detailed in Figure 2a, where is given the two simulation diagram implemented in MATLAB – Simulink ® simulation environment to control the AirFr based LF loop and FuelFr based sFF or ESC loop.

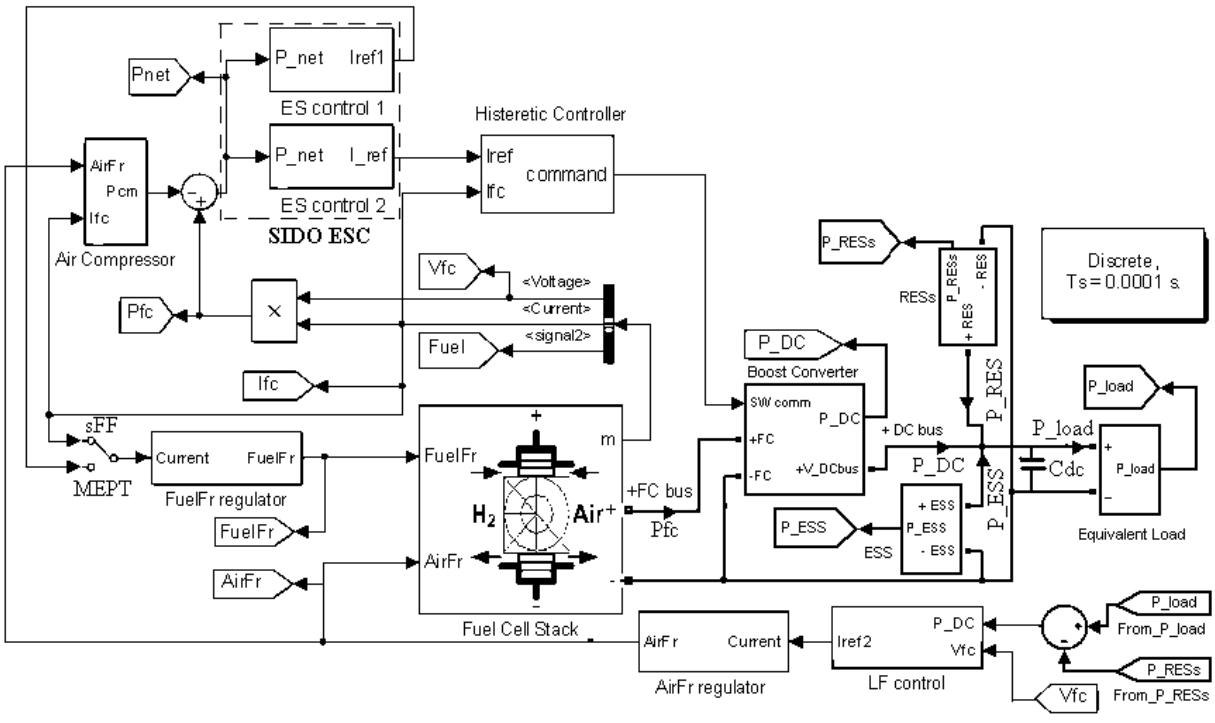

Figure 2a. The simulation diagram for Air-LF/Fuel-ESC and Air-LF/Fuel-sFF cases

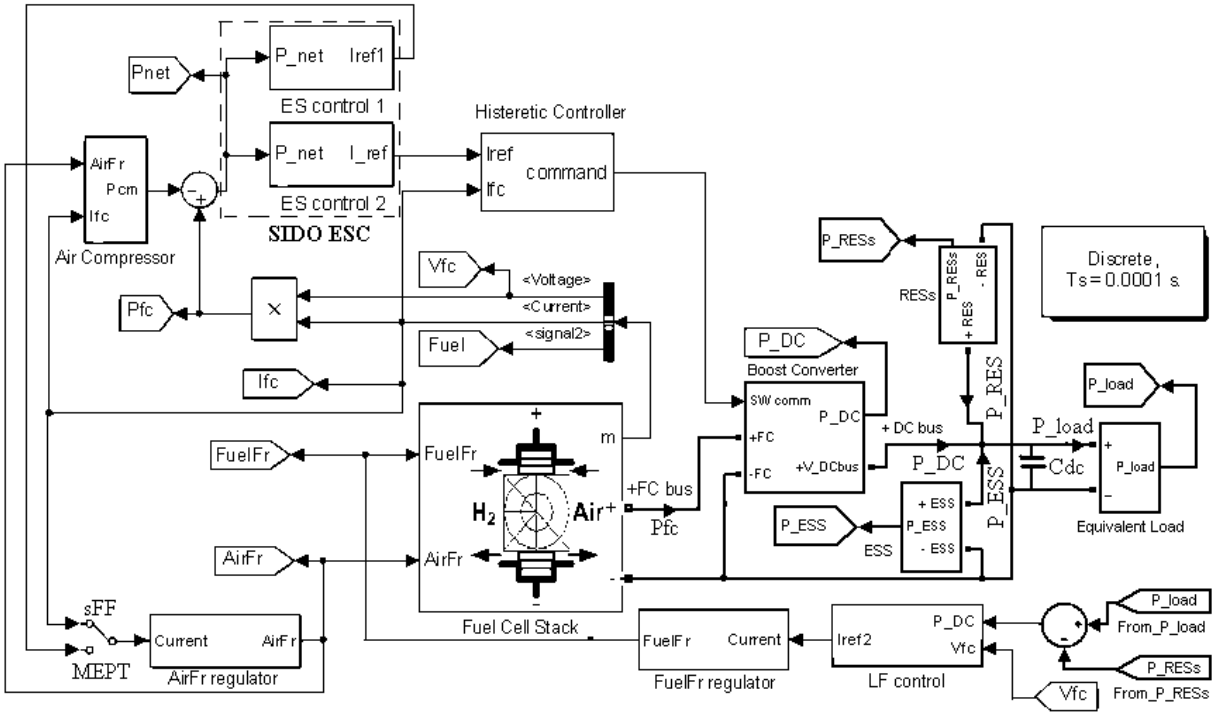

Figure 2b. The simulation diagram for Air-ESC/Fuel-LF and Air-sFF/Fuel-LF cases

Figure 2. The simulation diagrams for proposed EMU strategies to control the fueling rates

Other two control configurations to LF control the FuelFr are shown in Figure 2b, where the AirFr is sFF or ESC controlled. All four control configurations will be analyzed here.

The FC system must to operate efficiently, close to the maximum of the FC net power (named MEP). Different MEPT algorithm are proposed in the literature such as the ES control scheme [37], Perturb and Observe (P&O) method [48] or other type of searching algorithm [20, 49]. One MEPT algorithm will be implemented in the SIDO block to generate the both current references I_{ref} and I_{ref1}.

The voltage on DC bus could be chosen lower than 350-400 V if a bidirectional Z-Source Inverter (ZSI) is used to connect the AC loads [50]. Furthermore, the boost converter that interface the FC stack to DC bus will have a lower voltage ratio, being here implemented through a basic unidirectional boost topology. Thus, the DC voltage, u_{dc}, was set to 250 V on the DC bus, which is modeled as a capacitor, C_{DC} [51]. Consequently, the rated voltage of the rechargeable Li-ion batteries stack will be 250 V. The rated voltage of the ultracapacitors stack was chosen of 100 V. The bidirectional buck-boost converter interface the ultracapacitors stack to the DC bus, ensuring the dynamic power compensation on the DC bus. Linear and nonlinear control techniques can be used to regulate the voltage on the DC bus [46].

The reference current 2, I_{ref2}, is computed on LF control block based on the AV value of requested FC power on DC bus, $P_{Load} - P_{RES}$, considering that the AV value of the ESS power is zero (because the batteries stack operates in CS mode based on the LF control proposed here).

It is known that the dynamic FC response is dependent to the fueling rate, stoichiometric ratio, temperature, humidity and pressure [52]. Consequently, the fuel regulators must include a rate limiter to avoid the gas starvation [53] and a saturation block to operate the FC stack in available range of FC power. The minimum level of the FC power is set different to zero, avoiding the gas starvation that may appear during a repetitive start-up. So, the FC stack will operate in standby-mode at low fueling rates during the phases of low power demand, when RES power is higher that load demand. Consequently, the power flow balance on DC bus is a key relationship to design the EMU strategies [15,21,24,54].

3. The EMU strategies to control the fueling rates

Besides the power flow balance, which means acquisition of the all power flows (Figure 1), the other key decision parameters for the EMU strategies are the level of the FC and WT power, the state signals (such as SOC of the batteries and ultracapacitors stacks), the voltage on the FC and DC bus, the user signals (such as personalized prioritization of the loads into a smart home or environmental and internal ambient rules for the thermal comfort, rules to start the electrolyzer or charge the electrical vehicle, and so on), and the protection signals from and outside of the HPS.

Note that the main objective for all applied EMU strategies in the integrated HPS is to ensure the load demand. Consequently, the analysis performed in this paper is focused to show this based on the results obtained with the proposed LF and MEPT control loops, without considering the EMU meta-rules based on other key decision parameters mentioned above.

For example, the operating meta-rule for the hydrogen production via water electrolysis depends on the excess or shortage of power from the RES in comparison with the load demand, the SOC level of the batteries stack, the level of hydrogen in the storage tank of SOC. Implementation of such meta-rule based on the concept of Hierarchical Control Theory [31-32], which is mainly applied in integrated hybrid systems to schedule the operation of the involved subsystems based on a predefined hierarchy made on the decision flow [27], could be simple if the RES power flow is constant or varying slowly during a load cycle. The huge variability of RES power on the DC bus and random behavior of the load demand in a smart home increase the complexity of the EMU [25-26]. Furthermore, frequent start-up and shut-down actions for the FC stack and electrolyzer may degrade their life cycle [32,55]. Therefore, the EMU strategy based on LF control that continuous operates the FC is proposed here. The capacity of the batteries stack that operates in CS mode will be designed at minimum value needed to compensate the short-term variability of the RES power and sharp peaks of the random load demand. Thus, the batteries' lifespan is improved and the cost of the batteries stack is substantially reduced, and subsequently these influence the operating and maintenance costs of the entire HPS.

The MEPT control is proposed here to improve the energy efficiency of the entire HPS based on control of the fueling rates for the FC stack. Thus, the efficiency of the fuel consumption (or shortly the fuel efficiency) is improved. In brief, the EMU strategy proposed here based on efficient control loops aims to ensure the HPS operation under variable weather conditions and random load demand, maintaining the operating costs at a reasonable level.

The power flow balance on the DC bus is given by:

$$C_{dc}u_{dc}du_{dc}/dt = p_{RES} + \eta_{boost}p_{FCnet} + p_{ESS} - p_{Load} \quad (1)$$

where p_{RES}, p_{FCnet}, p_{ESS}, and p_{Load} are the power level of the RESs, FC system, ESS, and equivalent load, and η_{boost} is the energy efficiency of the boost converter. The AV value of (1) during a drive cycle is given by:

$$0 = P_{RES} + \eta_{boost}P_{FCnet} + P_{ESS} - P_{Load} \quad (2)$$

The LF control will assure P_{ESS}=0 during a drive cycle. So, the batteries stack will operate in CS mode, and (2) will give the AV value of the FC current:

$$0 = \eta_{boost}P_{netFC} + P_{RES} - P_{Load} \Rightarrow I_{FC(AV)} = (P_{Load} - P_{RES})/(V_{FC}\eta_{boost}) \quad (3)$$

The value given by (3) is the reference current 2, I_{ref2}, the output of the LF control block. The battery SOC is maintained in the desired range by the EMU meta-rules that, for example, start the electrolyzer or charge the electrical vehicle.

In brief, all HPS topologies proposed in this paper (Figure 2) are based on an MEPT and LF control loops that generate the reference currents, I_{ref}, for the boost controller, and I_{ref1} and I_{ref2}, for the FuelFr and AirFr regulators, respectively. The I_{ref} current is used in all control configurations to harvest the maximum of the FC net power available for the fueling rate set by each EMU strategy. The I_{ref1} current is used to control the FuelFr regulator (Figure 2a) or the AirFr regulator (Figure 2b), instead of the I_{ref2} current is used to control the AirFr regulator (Figure 2a) or the FuelFr regulator (Figure 2b). If I_{FC} current is used to control the FuelFr regulator (Figure 2a) or the AirFr regulator (Figure 2b), instead of the I_{ref1} current, then other two fueling control configurations will be obtained based on the sFF control scheme.

After the start-up procedure, all control configurations will be compared considering the following performance indicators [56]: (1) the fuel consumption, and (2) fuel efficiency.

The FC stack is fueled based on the levels of the RES and load power, considering (3), and the I_{ref} and I_{ref1} currents. The last two reference currents are generated by the SIDO ES controller that is detailed in [37] and briefly presented here. The stationary values of the fueling rates are tracked fast with good transitory accuracy and about 99.9% stationary accuracy. The fueling rates will be computed during a load cycle based on the real time optimization algorithm presented here under variable weather conditions and random load demand. The FC power requested on the DC bus, which is given by (3), will be tracked with limited slopes to avoid gas starvation. The results will show that the power difference is dynamically compensated by the ESS to satisfy the power flow balance (1). The search speed of the proposed ES control scheme can be easily set higher through the control parameters, up to the safe slopes recommended for the FC power profile [52,53]. Further contributions will be highlighted in Conclusion section based on the results obtained.

4. Modeling of the Standalone Renewable/Fuel Cell Hybrid Power Source

4.1. Fuel cell system

The PEMFC is the best option to be used as backup energy source in HPS because of its eco-friendly operations and high-energy density of the hydrogen. Thus, the RES/FC HPS can be driven indefinitely by refueling the hydrogen storage tank via the water electrolyzer that is supplied when the RES power exceed the load demand. Despite the disadvantages above mentioned, the PEMFC has also significant advantages such no emissions, low operating temperature, high efficiency, and short response to power demand [52,53] Furthermore, year by year, the cost of the PEMFC system decreases to competitive prices [51]. The auxiliary components are supplied by the FC stack, so the FC net power is given by (4):

$$p_{FCnet} = p_{FC} - p_{aux} \tag{4}$$

where p_{FC} is the power generated by the FC stack and p_{aux} is the power consumed by the auxiliary components.
The PEMFC system is a complex system, so a lot of research was performed in this direction of understanding and modeling of the PEMFC system [20]. The 6 kW/45V PEMFC model included in the SimPowerSystems library of the Matlab - Simulink® will be considered here [57]. The FC net power characteristic for nominal value of the fueling rates and main FC parameters are shown in Figure 3. The zoom shows that in the case of rated fueling the MEP is about 5400 W. It is obvious that the MEP will have different position in the FC net power – FC current phase plane during the operation of the RES/FC HPS under the variability of both RES and load power flows. The MEP is difficult to be tracked in real-time considering the mass transport processes and different dynamics of the auxiliary components that change the behavior of the overall system. Consequently, the p_{FCnet} is necessary to be tracked based on adaptive MEPT control scheme, such as the advanced ES control scheme proposed in [36,37].
Because the air compressor is the main power consumer among the auxiliary components, the variability of p_{aux} power is modeled here only by the power consumed by the air compressor power (which is up to 80% from p_{aux} power [58]). The effect of the thermal management can be neglected in comparison with the time constants of the PEMFC stack and air compressor [59]. The compressor model is shown in Figure 4 and the power of the air compressor, P_{cm}, is computed based on (5) [39,48].

$$P_{cm} = I_{cm} \cdot V_{cm} = \left(a_2 \cdot AirFr^2 + a_1 \cdot AirFr + a_0\right) \cdot \left(b_1 \cdot I_{FC} + b_0\right) \tag{5}$$

where $a_0 = 0.6$, $a_1 = 0.04$, $a_2 = -0.00003231$, $b_0 = 0.9987$, and $b_1 = 46.02$.
The compressor dynamics is modeled through a 2nd order system [39] or a dynamic system of higher order [48]. The power of the air compressor is set in the power range through the static gain, the P_{cm} power being about 1 kW for a gain of 0.45.
The fueling regulators are also shown in Figure 4. Each regulator includes a rate limiter and saturation block, having a protection role that was already mentioned. The FuelFr and AirFr values are given by:

$$FuelFr = \frac{60000 \cdot R \cdot \left(273 + \theta\right) \cdot N_C \cdot I_{ref(H2)}}{2F \cdot (101325 \cdot P_{f(H2)}) \cdot (U_{f(H2)} / 100) \cdot (x_{H2} / 100)} \tag{6}$$

$$AirFr = \frac{60000 \cdot R \cdot \left(273 + \theta\right) \cdot N_C \cdot \cdot I_{ref(O2)}}{4F \cdot (101325 \cdot P_{f(O2)}) \cdot (U_{f(O2)} / 100) \cdot (y_{O2} / 100)} \tag{7}$$

where:
R = 8.3145 J/(mol K);

F = 96485 As/mol;
N_C represents the number of cells in series (65);
θ - operating temperature (65^o Celsius)
$U_{f(H2)}$, $U_{f(O2)}$- nominal utilization of hydrogen (99.56%) and oxygen (59.3%);
$P_{f(H2)}$, $P_{f(O2)}$- pressure of the fuel (1.5 bar) and air (1 bar);
x_{H2}, y_{O2}– composition of fuel (99.95%) and oxidant (21%);
$I_{ref(H2)}$, $I_{ref(O2)}$- reference currents.
The reference currents are generated by the SIDO ES (I_{ref1}) and LF (I_{ref2}) control schemes: $I_{ref(H2)} = I_{ref1}$ and $I_{ref(O2)} = I_{ref2}$ in Figure 2a, and vice versa in Figure 2b, where $I_{ref(H2)} = I_{ref2}$ and $I_{ref(O2)} = I_{ref1}$. If the sFF control is applied to FuelFr or AirFr regulaters, then $I_{ref(H2)} = I_{FC}$ (Figure 2a) or $I_{ref(O2)} = I_{ref2}$ (Figure 2a). If both FuelFr and AirFr are regulated through the FC current based on (6) and (7), then the classical sFF control is applied [60].
The surface of the FC net power is shown in Figure 5 through the contour lines obtained for different FC currents. The FC nominal parameters are also mentioned in Figure 5.

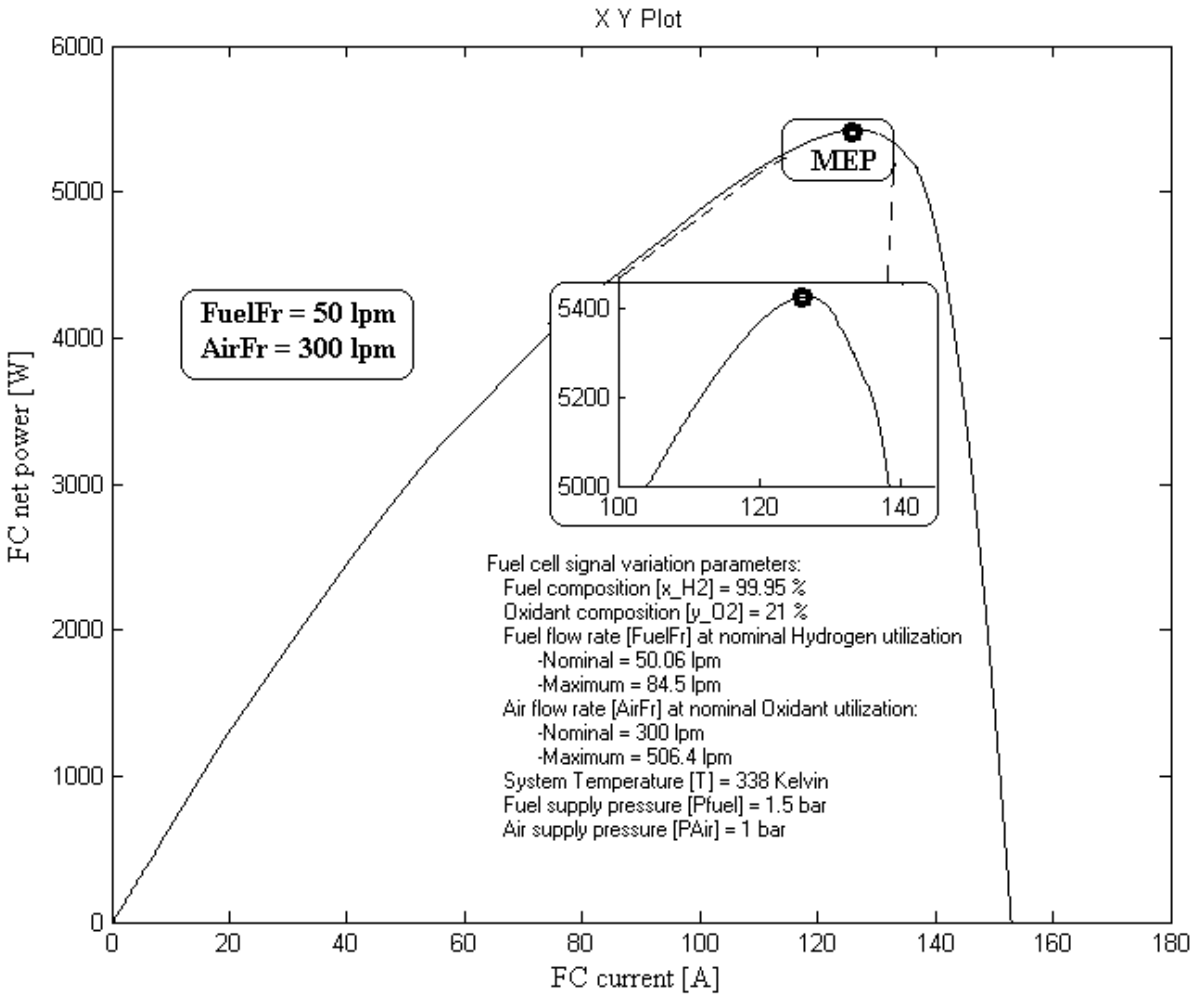

Figure 3. The FC net power characteristic for the nominal values of fueling rates

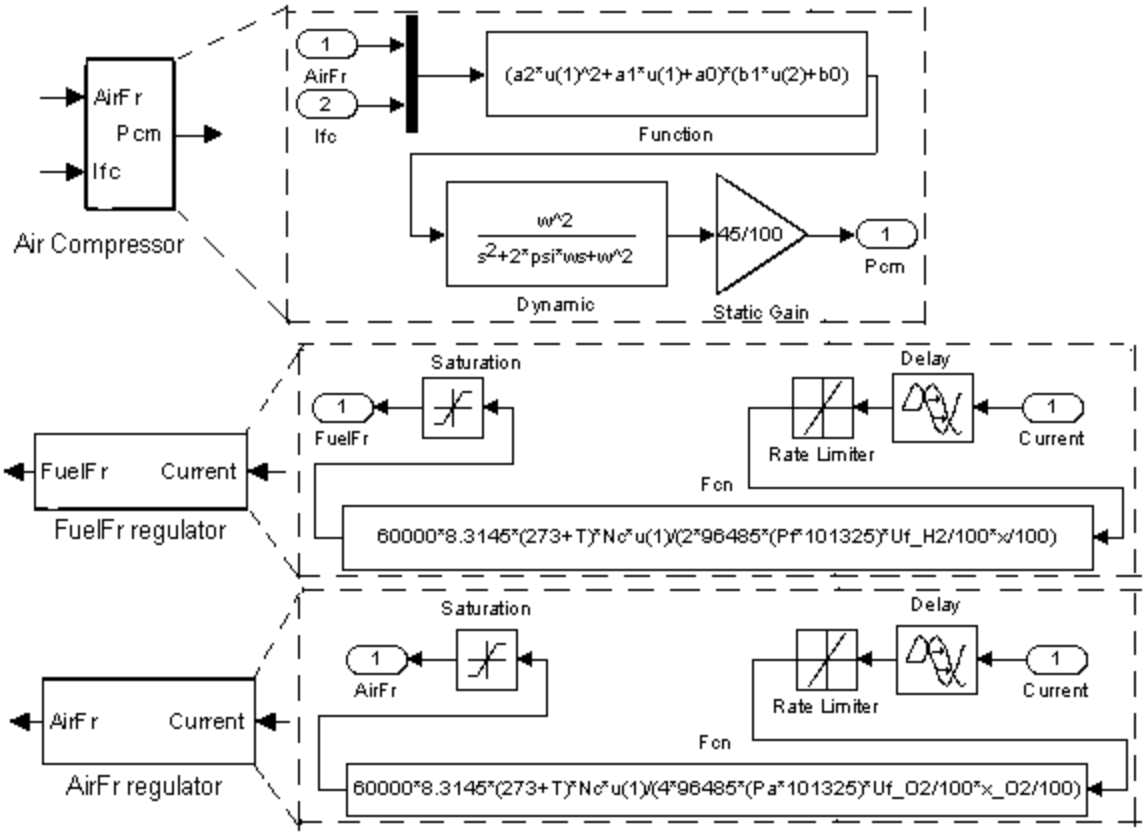

Figure 4. The diagrams of the FC system components (AirFr and FuelFr regulators and air compressor)

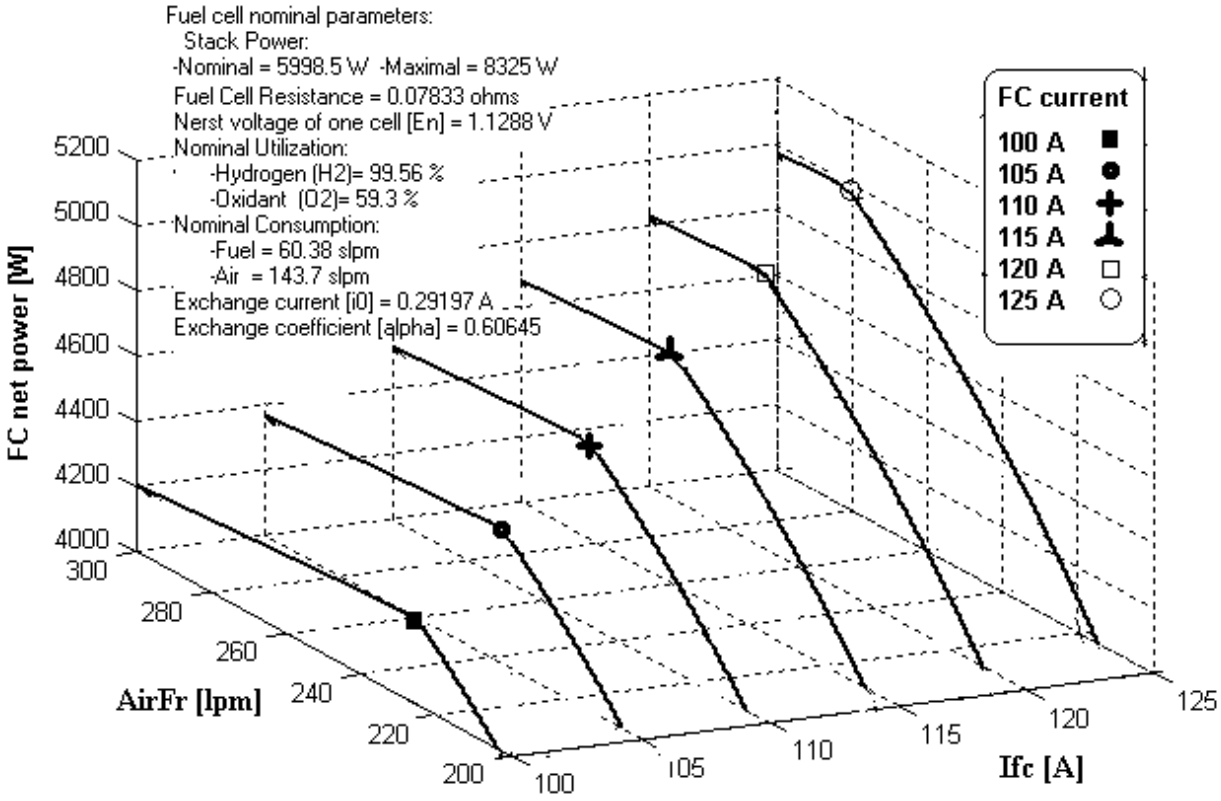

Figure 5. The FC net power surface

4.2. Renewable energy sources

RESs have a lot of advantages including sustainability, reduction of carbon dioxide, and economic benefits, but the intermittent nature and low efficiency of many RESs request to be integrated into a RES HPS [10,19,24].

For example, the WT and PV energy resources in a given area can be complementary in a certain period of time [26]. A generic model of any combination of RESs is used in this paper in order to test the control topologies proposed under a RES power profile close to real one (Figure 6). Thus, two power sequences define the PV and WT power profiles without random fluctuations. The variability of the RES power profile is added randomly based a random sequence. A RES power profile is shown in Figure 6 for a sunny day with some clods at noon and afternoon, and moderate wind in the evening. The peak of the RES power profile is of 5 kW, close to the peak of the load demand for a smart home. Nevertheless, because these peaks of the PV and WT power profile are not synchronized, a backup energy source is usually used [30,31].

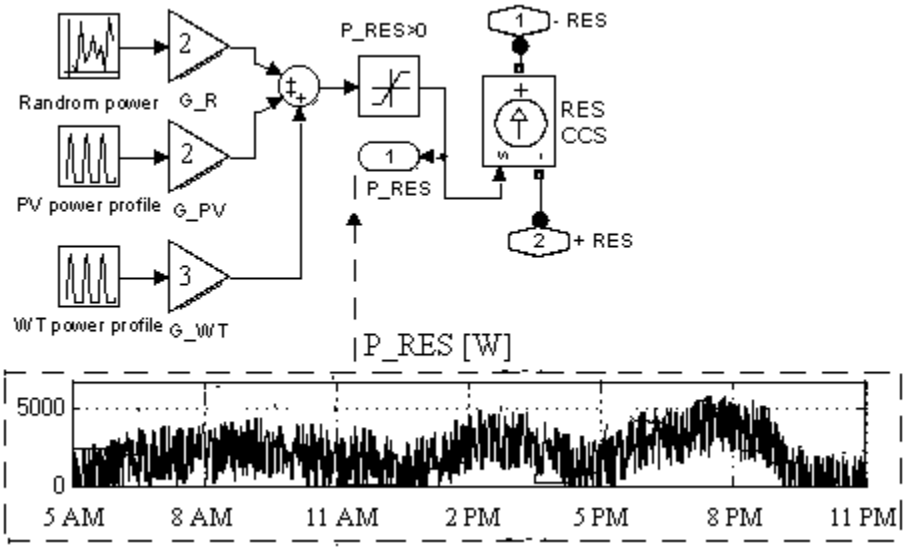

Figure 6. The diagram of the RES model

4.3. Energy Storage System

The hybrid batteries/ultracapacitors ESS is necessary to ensure the power flow balance (1) under unknown RES power profile and random load demand. The hybrid semi-active topology for the ESS is used here to evaluate the impact of adding ESS on the performance of a RES HPS [47]. The ESS is charged during an energy surplus on the DC bus (RES power higher than load demand and FC system operates on standby mode), when the electrolyzer can be started depending of the battery SOC. The ESS is discharged a bit during step-up load until the FC system starts to operate in the LF control loop. Thus, the deep-discharge cycles are avoided if the LF control is implemented to fuel the FC stack. This number of deep-discharge cycles is limited for all types of batteries, but it is practically unlimited for the ultracapacitors stack. Consequently, the voltage regulation on the DC bus is ensured by appropriate control of the bidirectional DC-DC converter that interface the ultracapacitors stack to the DC bus.

The batteries stack is connected directly to the DC bus in the hybrid semi-active ESS topology (see Figure 7) used here to operate the batteries stack in CS mode through the LF control proposed. The ultracapacitors stack is connected to the DC bus via a bidirectional DC-DC converter in order to decrease the number of ultracapacitor cells, assures a large range for the ultracapacitor SOC, and achieve an active control of DC bus voltage [23]. Thus, the FC system and ultracapacitor stack operate as active controlled power sources. The batteries stack operates as passive controlled energy sources assuring the power flow balance (1).

In this paper, the generic model of the lithium-ion battery included in the SimPowerSystems library of the Matlab - Simulink® is used [57]. The nominal voltage, rated capacity and initial SOC were set at 250 V, 100 Ah and 80%. The preset battery parameters have been computed depending on battery type and rating values. Different battery sizes are also used in simulation, according to the EV33 rule [61]. The power flow balance on the DC bus is dynamically compensated by the ultracapacitor stack. Different ultracapacitor models have been proposed based on electric [62] and non-electric models [63]. The last class of models uses a controlled current source to be connected to the electrical circuit and a computational algorithm to evaluate that current. The electrical models have the disadvantage of direct connection to the bidirectional buck-boost converter (see

Figure 7). The classical electric circuit model, which includes the equivalent series and parallel resistors (ESR and EPR), and a capacitor (C), will be used in this paper. The initial voltage, C, ESR and EPR have been set at 100 V, 100 F, 0.1 Ω and 10 kΩ.

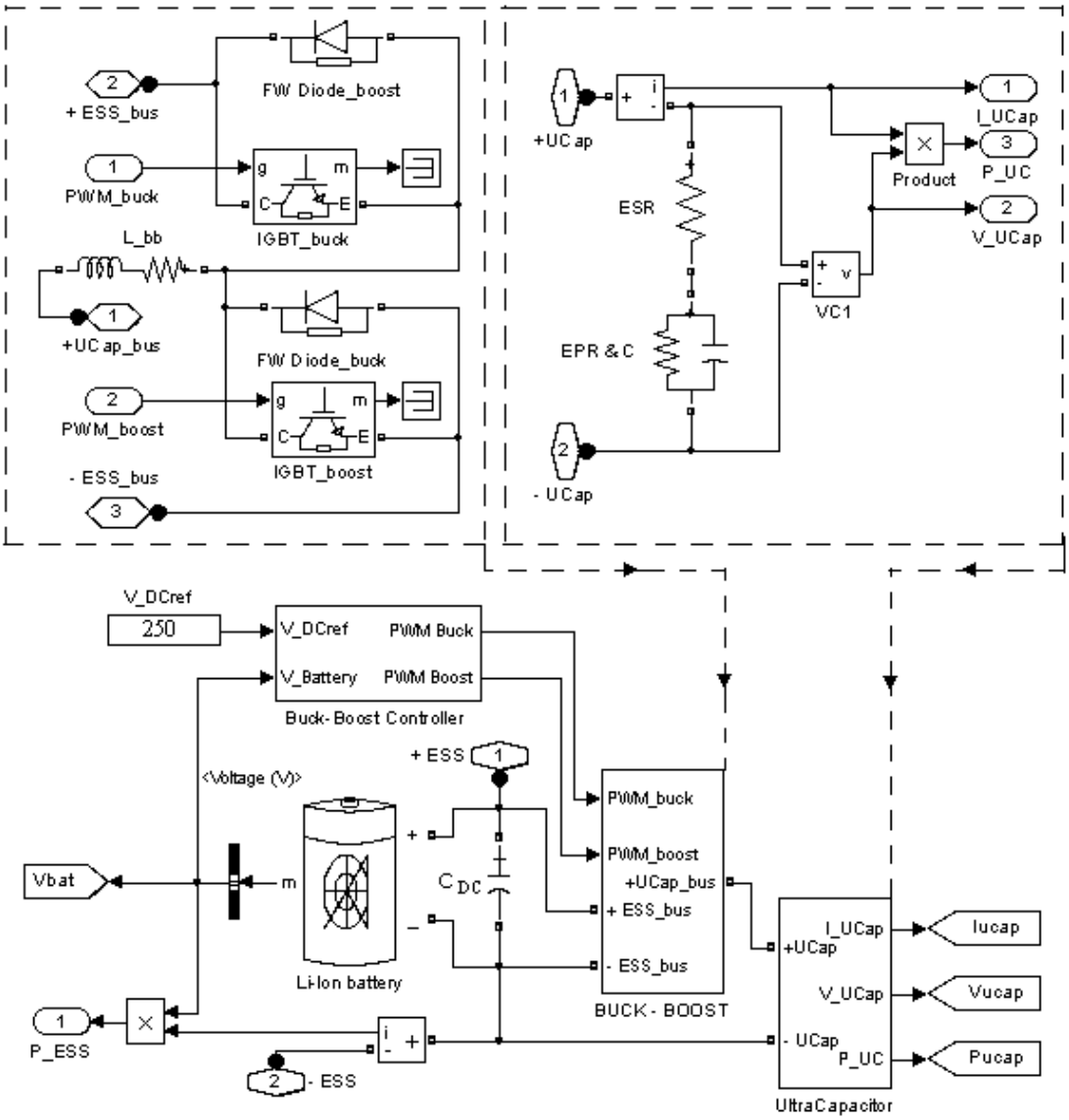

Figure 7. The diagram of the ESS model

4.4. Power interfaces

Power interfaces are needed to effectively adapt the RES voltages to DC voltage based on MPPT controller that uses a current or voltage reference. The reference is used in the PWM control of the respective power interface. For example, an AC-DC and DC-DC power converter is necessary to interface the WT and PV systems. The FC system is interfaced through a DC-DC power converter that is MEPT controlled. If multi-source HPS architecture is need to be designed, then multiport power convertor topology is recommended, instead of implementing several power converters. Furthermore, efficiency and cost are greatly enhanced because the number of passive and switching components is heavily reduced [40]. The DC power bus is the output of the multiport power convertor (see Figure 1). The AC loads are supplied from the DC bus via an inverter system. Multiport power convertor is directly fed by all energy sources available based on the optimized EMU strategy [65]. As it was mentioned in previous section, three DC-DC power converters are used to interface the FC, PV and ultracapacitors stack. The first two DC-DC power converters are of unidirectional type, adapting the FC and PV voltage to the voltage level set on the DC bus (250 V). For example, the unidirectional DC-DC power converter that interfaces the FC system is of boost type (see Figure 2) because the FC voltage is lower than 250

V, being in range of 40-65 V for a FC power variation from rated power to standby power level. The AV value of the FC power flow that supply the DC bus is dependent to energy efficiency of the boost converter:

$$P_{DC(AV)} = \eta_{boost} P_{netFC} \Rightarrow \eta_{boost} = P_{DC(AV)} / P_{netFC} \quad (8)$$

The energy efficiency of the boost converter is set here to 0.95.

The bidirectional buck-boost converter (see Figure 7) that interface the ultracapacitors stack is controlled to stabilize the DC voltage at V_{DCref} = 250 V. The switching model uses the following components from the SimPowerSystems® [57]: a high-frequency inductor (L_{bb}), an output filtering capacitor on DC bus (C_{DC}), two flywheel diodes, and two IGBT switches.

4.5. The equivalent load

The equivalent load modeling must to cover the DC and AC loads, which depends to particular HPS application. For example, the power consumption pattern for a smart home is random even the EMU strategy can schedule the priority of load connection [2]. Modeling the equivalent load by analyzing each and every AC and DC load structure and behavior is quite difficult and it is outside of the goal of this paper. Nevertheless, experimental test failures can be avoided by adequately modeling of the power load profile based on loads specifications, and appropriate adaptive load dispatching and forecasting strategy [3]. The load power profile is usually set using two main approaches [12,27]: component-based and measurement-based. The first method requires detailed information on AC and DC loads composition and data-sheet specifications, while the second is based on the experimental-test approach in modeling the load power profile.

The load profile must to highlight the variations in power demand during a load cycle (a day, month or a season). Design of standalone HPS requires appropriate load power profile to analyze the balance between energy demand and supply, including optimal control of the power flows with the help of advanced metering technologies available in the smart home. It is known that 10-30% domestic energy consumption reduction can be accomplished by only providing the load power profile to the users, helping them to change their behavior [65].

So, the load power profile is set based on the diagram of the dynamic load shows in Figure 8.

Two operating regimes can be set: the constant load, if the switch is on the I_{LoadDC} position, and the dynamic load, if the switch is on the load current sequence. A random profile can be added in both regimes. The equivalent load is modeled as a controlled DC current source.

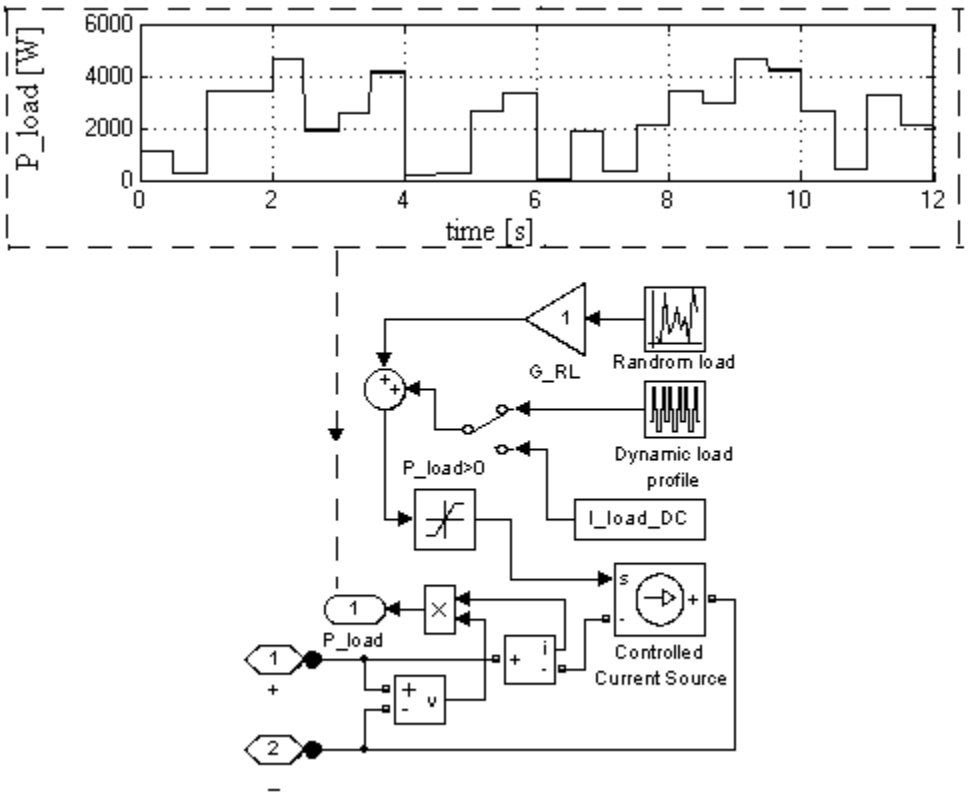

Figure 8. The diagram of the dynamic load

In this work, different load power profiles were used in order to evaluate the performance indicators: fuel consumption and fuel efficiency.

5. The Energy Management Unit

The EMU strategy must to mitigate the effects of the RES variability under different weather conditions based on a proper design of the HPS topology to assure cost reduction and minimizes the ESS size under different load demands. Demand Side Management approach is proposed as EMU strategy for reliable and economical supply of the load demand [1-3]. Shortly, Demand Side Management strategy ensure the load demand following by controlling the energy consumption of appliances and optimizing their operation at the user side, for instance, by scheduling the non-priority appliances from peak time to off-peak time [2].

The EMU strategies proposed here are based on integration of two control loops to regulate the fueling rates, which includes the SIDO ESC scheme [37] and LF controller [15] (Figure 9).

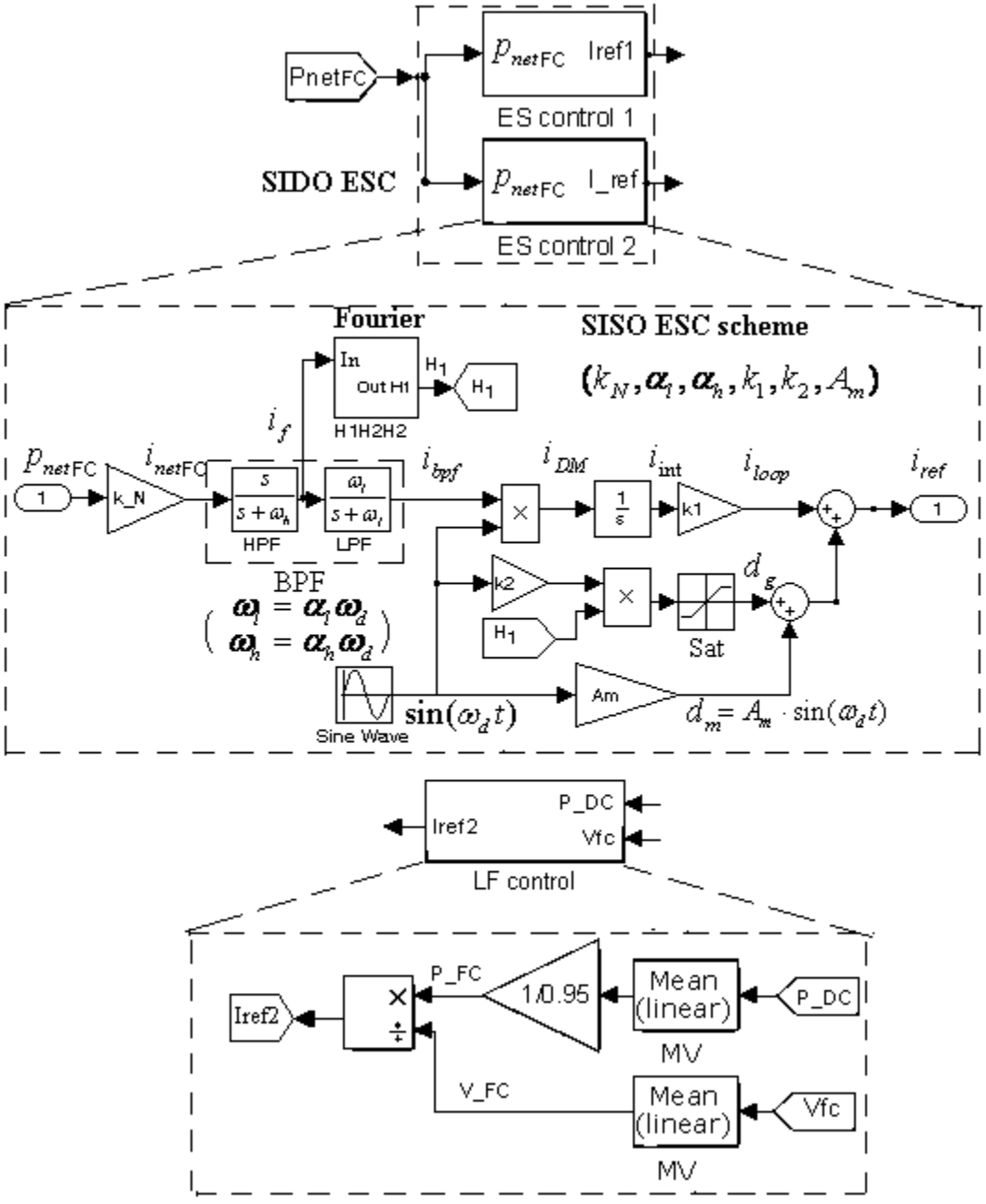

Figure 9. The diagrams of the EMU controllers (SISO ESC and LF control schemes)

5.1. The SISO ESC scheme

The diagram of the Single-Input Single-Output (SISO) ES control scheme is shown in Figure 9, and the equations are the following [36]:

$$i_{netFC} = k_N \cdot p_{netFC} \tag{9}$$

$$\dot{i}_{hpf} = -\omega_h i_{hpf} + \omega_h i_{netFC},\ i_f = i_{netFC} - i_{hpf},\ \dot{i}_{BPF} = -\omega_l i_{BPF} + \omega_l i_f,\ \tag{10}$$

$$i_{DM} = i_{BPF} \cdot \sin(\omega_d t) \tag{11}$$

$$\dot{i}_{\text{int}} = i_{DM} \tag{12}$$

$$i_{loop} = k_1 i_{\text{int}} \tag{13}$$

$$d_g = k_2 H_1 \sin(\omega_d t),\ d_m = A_m \sin(\omega_d t) \tag{14}$$

$$i_{ref1} = i_{loop} + d_g + d_m \tag{15}$$

where equations (9), (10), (11), (12), (13), (14) and (15) represent the FC net current, the band pass filter (including the i_{hpf} variable of the high-pass filter (HPF)), the modulator, the integrator, the gained variable in the ES loop, the H_1 - gained and the minimum dithers, and the current reference.

The following notations and values have been used in simulation:

$f_d = \omega_d/2\pi$ is the dither frequency (100 Hz)

k_1 - the ES loop gain ($k_1 = 4f_d = 400$);

k_2 - the dither gain (2);

k_N - the normalization gain ($k_N = 1/V_{FC} = 1/45$);

ω_l and ω_h - the cut-off frequencies of the band-pass filter (BPF), where $\omega_l = \alpha_l \omega_d$, $\alpha_l = 5.5$, and $\omega_h = \alpha_h \omega_d$, $\alpha_h = 0.1$;

H_1 - the magnitude of fundamental harmonic of the FC net current;

A_m - the minimum amplitude of the dither (0.001);

$*$ - the convolution operator.

The ESC optimization problem can be defined as:

Maximize:

$$P_{netFC} = J(x, I_{ref(H2)}, I_{ref(O2)}, I_{Load}) \tag{16}$$

Subject to:

$$\dot{x} = f(x, I_{ref(H2)}, I_{ref(O2)}, I_{Load}),\ x \in X \tag{17}$$

where $I_{ref(H2)}$ and $I_{ref(O2)}$ are the control inputs, I_{Load} is the disturbance input, and f is a smooth function that represents the dynamics of the FC stack based on states model. Note that the state vector, x, can be of a 9th [60] or 6th [66] order.

The second ESC scheme will use the orthogonal dither signal $s_{d2} = \cos(\omega_d t)$ in order to generate the I_{ref} reference current based on the same simulation parameters: $\omega_d = 2\pi \cdot 100$, $k_N = 1/45$, $\omega_h = 0.1\omega_d$, $\omega_l = 5.5\omega_d$, $k_1 = 4f_d$, $k_2 = 2$, $A_m = 0.001$.

5.2. The LF controller

The diagram of the LF controller is shown in Figure 9, too. The mean value of the input signal over a running window of one cycle of the dither frequency is computed here based on the AV blocks, but different other filtering techniques could be used as well. Thus, considering (3), the I_{ref2} reference current is estimated based on (18):

$$I_{ref2} = I_{FC(AV)} = (P_{Load} - P_{RES}) / (V_{FC} \cdot \eta_{boost(AV)}) \tag{18}$$

where $\cdot \eta_{boost(AV)}$ is set to 0.95.

The RES/FC HPS under the four EMU strategies proposed here to control the fueling rates have been tested for different load power profiles by using MATLAB-Simulink®.

6. Case studies and discussions

Three case studies are considered to evaluate the performance of the EMU strategies proposed for the RES/FC HPS: constant load, random pulsed load, and variable load under different RES power profiles. The

performance indicators used are the fuel consumption (F), which means the liters of fuel consumed during a load cycle, and fuel efficiency, which means the net energy generated by the FC system under different EMU strategies during a load cycle.

6.1. Constant load

The FC net power generated is different for the simulation diagrams shown in Figure 2, even the load is constant (see the left columns of Table 1). This is because different MEPs were tracked in the LF control loop and ESC (or sFF) control loop (see the levels of the AirFr and FuelFr values in Figure 10).

Table 1. The results to step load for the simulation diagrams shown in Figure 2

Diagram / I_{load} [A]	FC net power, P_{netFC} [W]						Fuel consumption, F [l]						Fuel efficiency [J/l]					
	5	10	15	20	25	30	5	10	15	20	25	30	5	10	15	20	25	30
Air-LF/ Fuel-ESC	1613	3131	4309	5318	6131	6850	32.54	70	99.68	125.34	144.08	167.62	558.5	497.45	474.25	461.6	450.6	440.9
Air-ESC/ Fuel-LF	793.6	2003	3205	4152	5157	6064	22.71	47.66	73	100.56	130.48	166.56	**467.6**	509.5	499.45	467.2	432.35	396.1
Air-LF/ Fuel-sFF	1588	2925	3989	4874	5674	6639	39.22	75.84	105.44	130.78	156.68	203	480.35	453.3	440.45	430.05	413.95	363.8
Air-sFF/ Fuel-LF	1306	2553	3699	5442	5886	6836	25.5	54.66	83.86	117.44	155.5	199	596.5	556.5	526.5	487.75	446.5	403.6

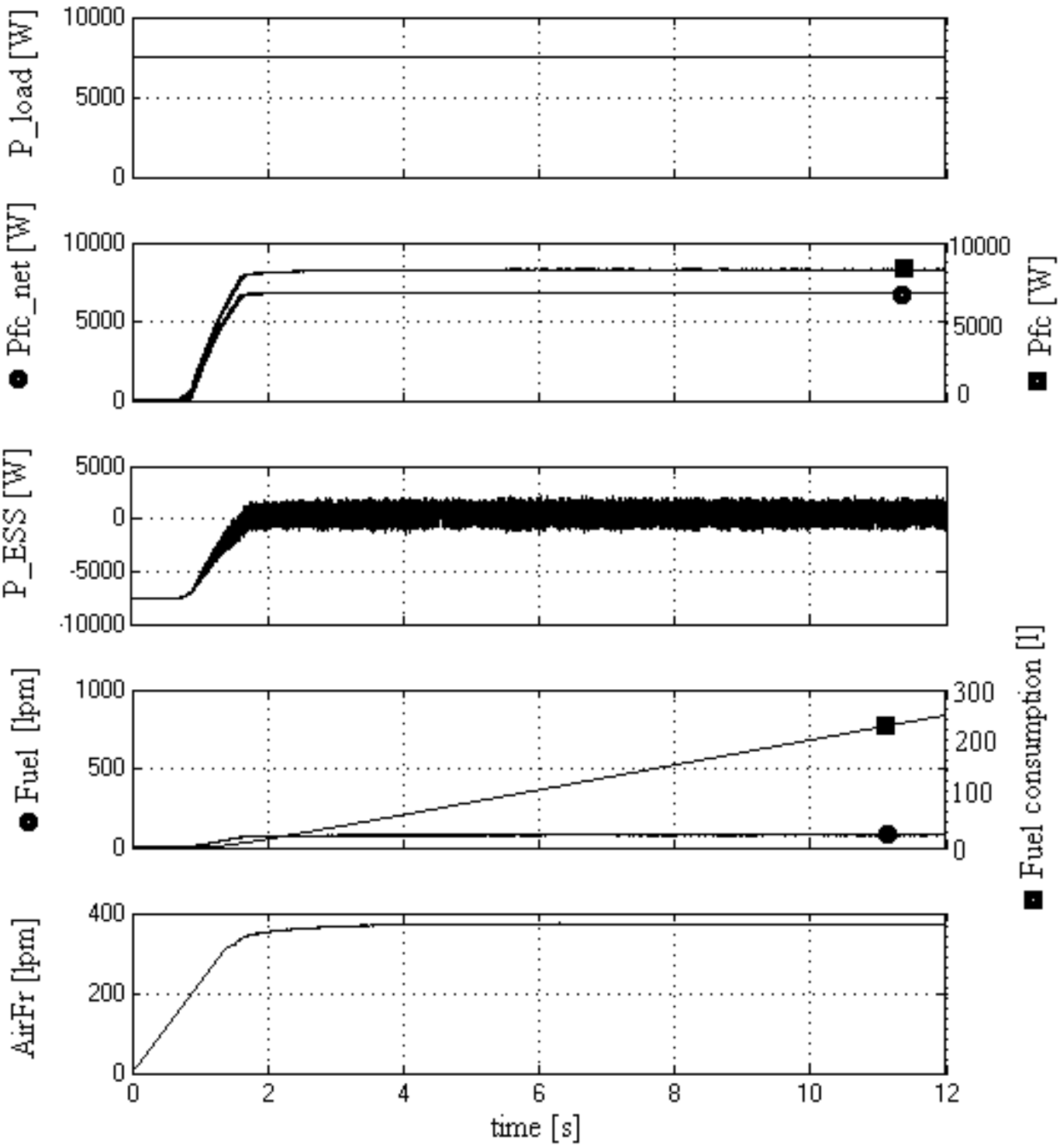

Figure 10a. The results for the Air-LF/Fuel-ESC simulation diagram

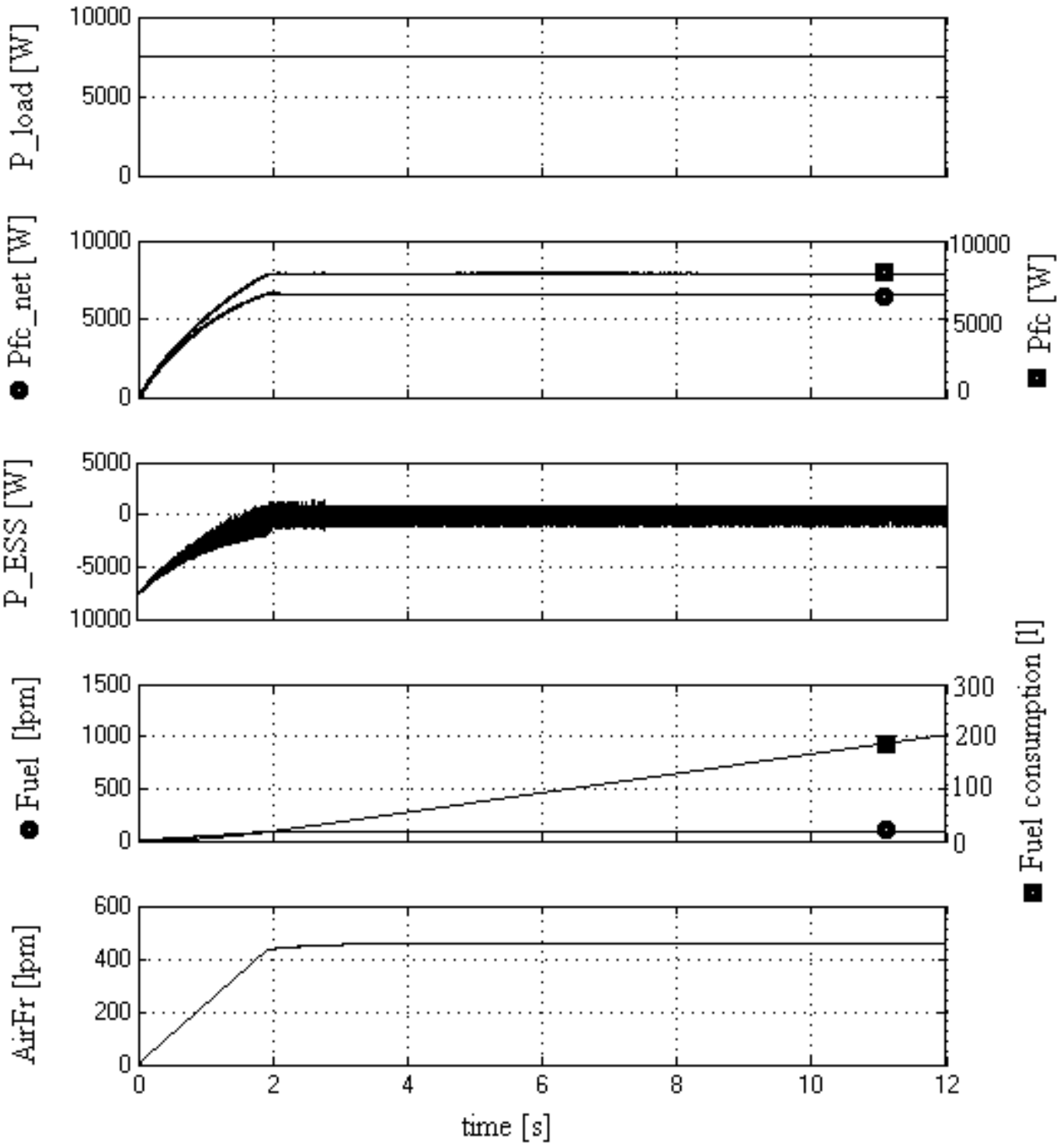

Figure 10b. The results for the Air-LF/Fuel-sFF simulation diagram

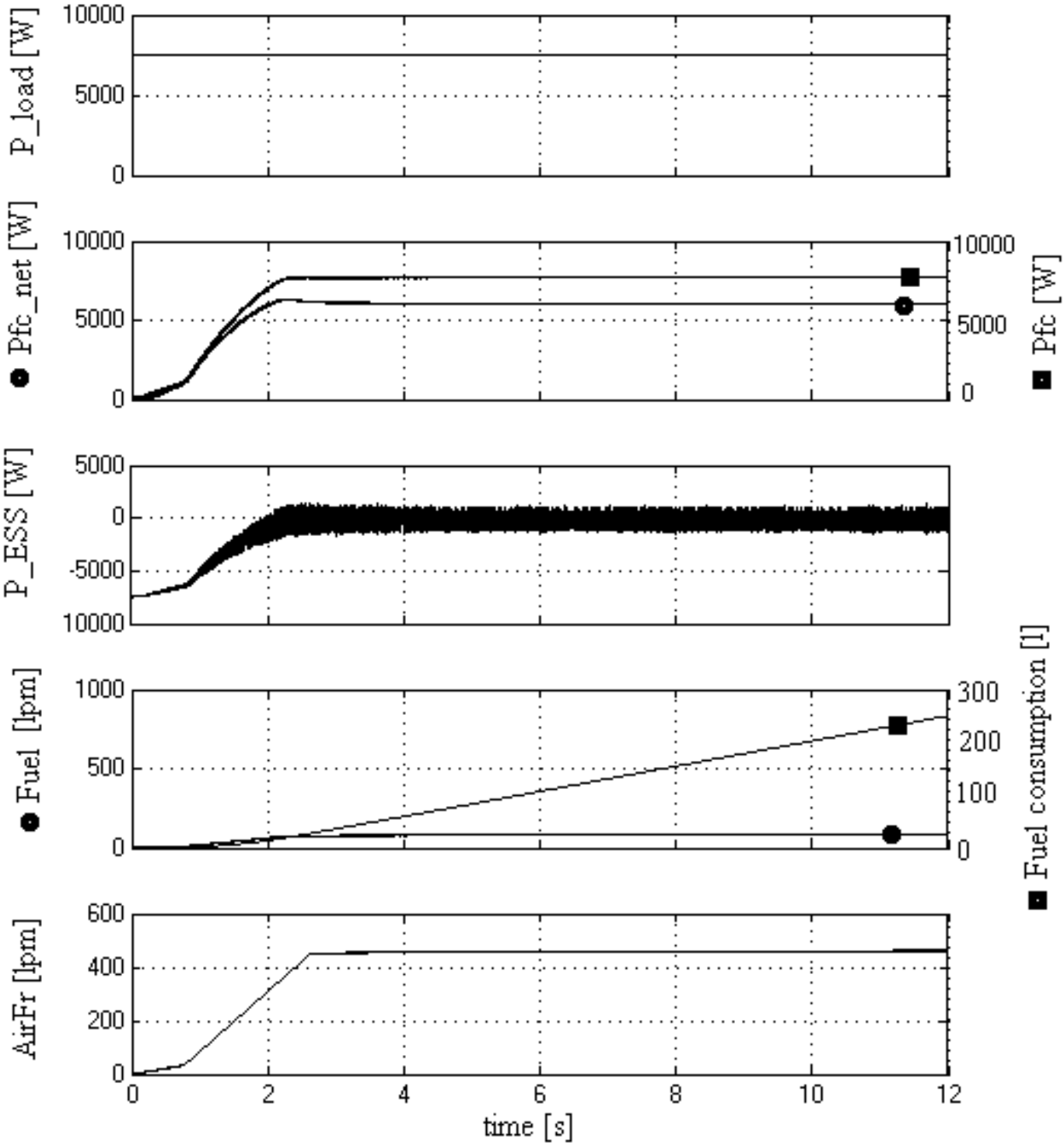

Figure 10c. The results for the Air-ESC/Fuel-LF simulation diagram

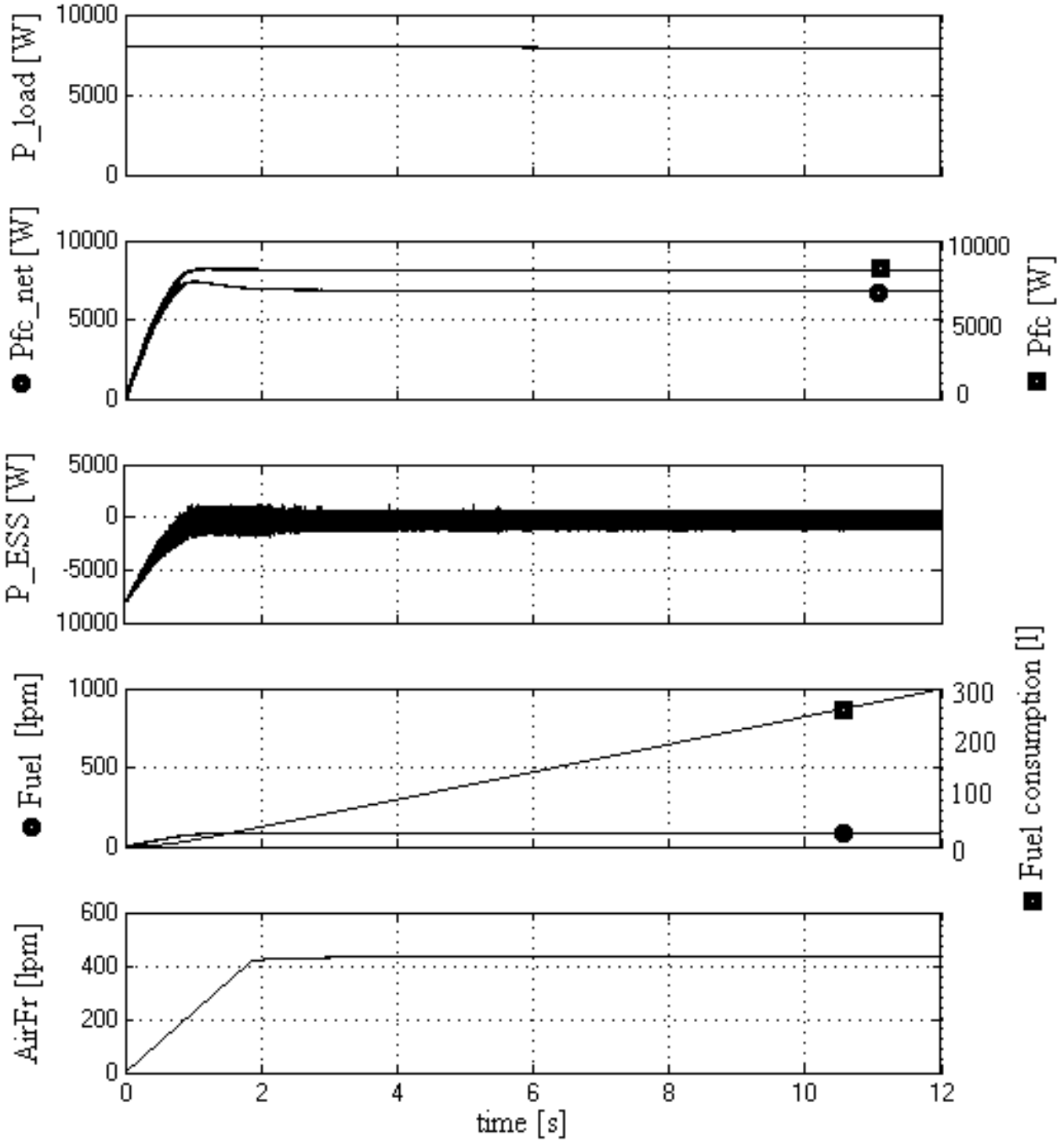

Figure 10d. The results for the Air-sFF/Fuel-LF cases simulation diagram

Figure 10. The results to step load for the simulation diagrams shown in Figure 2

The fuel consumption is also different, being minimum for the Air-LF/Fuel-ESC and Air-ESC/Fuel-LF control topologies (see the middle columns of Table 1) if the load current is of 30 A. The best control topology to minimize the fuel consumption seems to be the Air-ESC/Fuel-LF control topology (see the right columns of Table 1). So, this control topology should be used if the control goal is to minimize the fuel consumption (for example in some control strategies used in FC vehicle). If the control goal is to maximize the FC net power generated for a given level of the fuel consumption (which means to maximize the fuel efficiency indicator),

then the Air-LF/Fuel-ESC and Air-sFF/Fuel-LF control topologies should be used (see the right columns of Table 1). For all control topologies it can be noted that the values of the fuel efficiency indicator decreases with the increase of the load level. The exception value that is bolded in Table 1 appears because the searching value of the AirFr is limited to the maximum value of 500 lpm, so the MEP cannot be tracked. Also, note that the Air-LF/Fuel-ESC control topology is efficient for high load (around the load values that require FC net power close to rated value) and Air-sFF/Fuel-LF topology for light load.

The fuel efficiency indicator is shown in Figure 11 for a load current of 30 A. The values at 12 seconds are shown in Table 1. Note that the stationary value is reached until 24 seconds and the values mentioned in Table 1 for the Air-ESC/Fuel-LF control topology decreases most in comparison with the other control topologies.

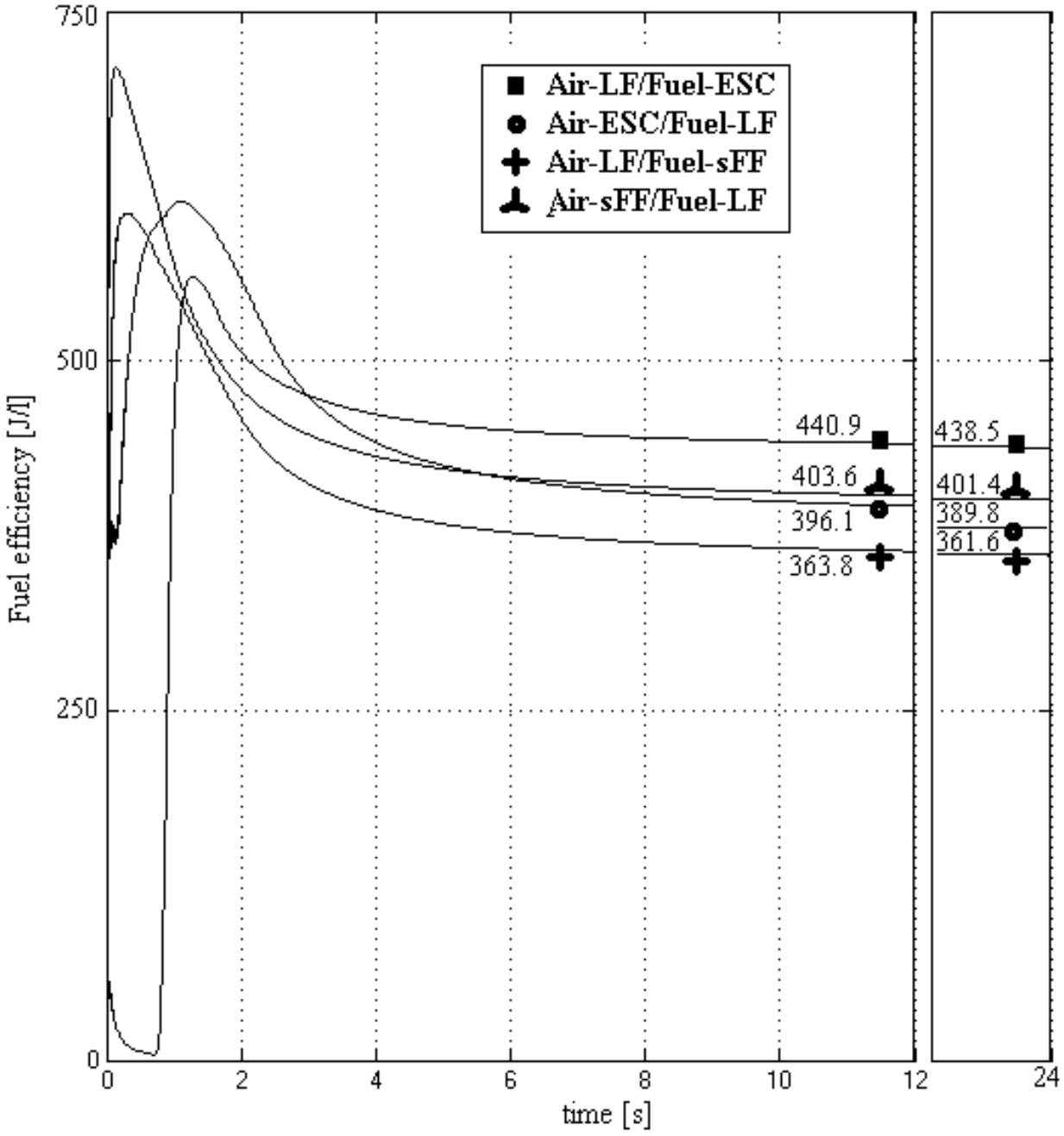

Figure 11. Fuel efficiency indicators for the simulation diagrams shown in Figure 2

For the autonomous FC HPS the goal is to maximize the fuel efficiency indicator, so these control topologies must to be further investigated.

Anyway, it is clearly that all control topologies based on LF control loop operates the batteries stack in CS mode (see the third plot in Figure 10). Also, in all cases, the MEP is tracked, the FC net power being in range of 10 to 20% from the FC power generated (see the second plot in Figure 10).

6.2. Random pulsed load

The FC response for Air-LF/Fuel-ESC control topology under random load is shown in Figure 12. The ESS makes face to random pulsed load in order to assure the power flow balance on DC bus, operating during a load cycle in CS mode (see the third plot in Figure 12). The FC response for all control topologies are almost the same.

The fuel efficiency indicators are shown in Figure 13 for Air-LF/Fuel-ESC and Air-sFF/Fuel-LF control topologies. It can be noted that best value of efficiency indicators depends to load level (as it was shown in Table 1) and the Air-LF/Fuel-ESC control topology is efficient for high load and Air-sFF/Fuel-LF control topology for light load.

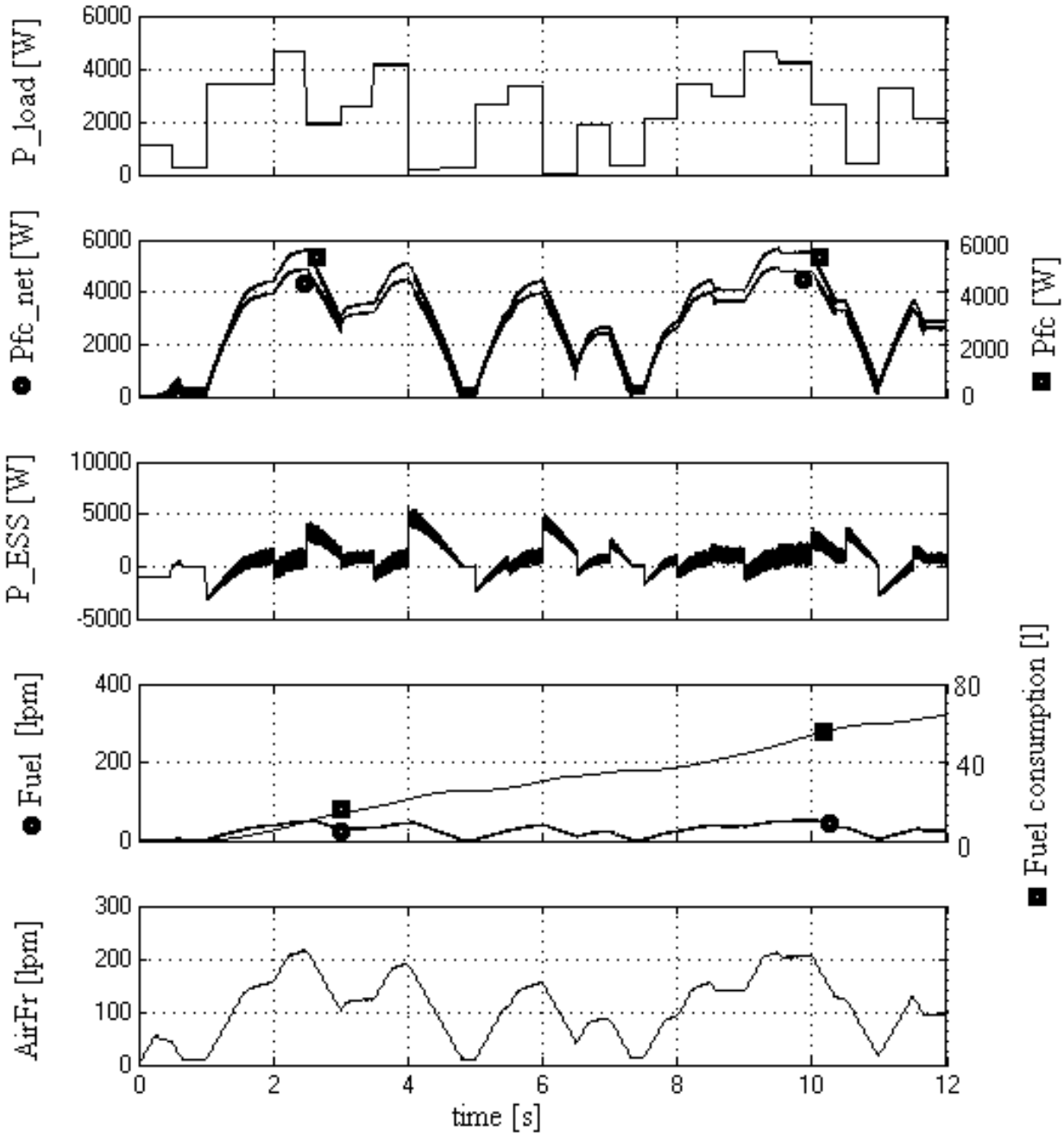

Figure 12. The FC response for Air-LF/ Fuel-ESC control topology under random load

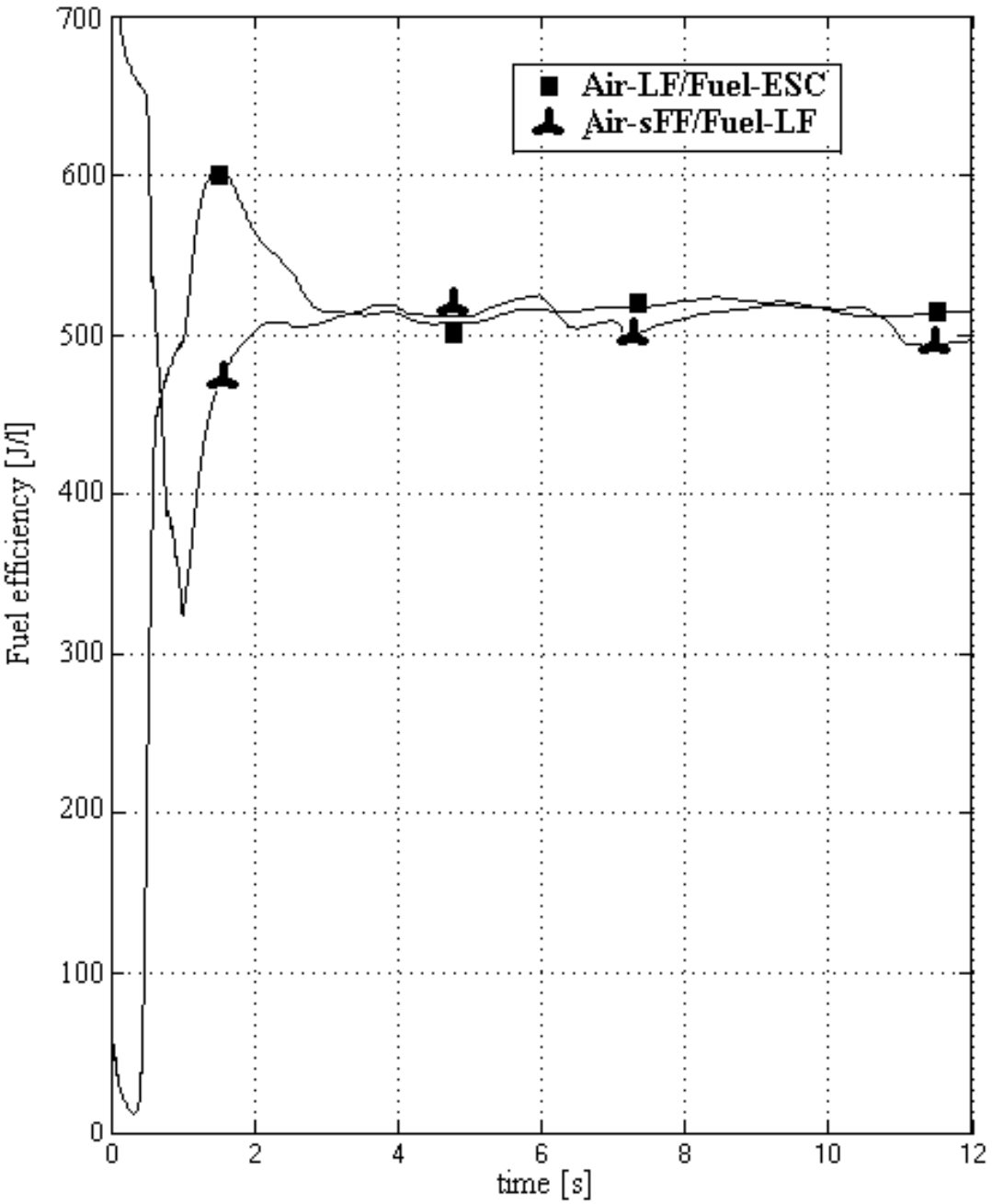

Figure 13. Fuel efficiency indicators for Air-LF/ Fuel-ESC and Air-sFF/ Fuel-LF control topologies

6.3. Variable load under different RES power profiles

A variable load profile is proposed in Figure 14 for a residential home from 5 AM to 11 PM, which will be ruled during 12 seconds of simulation. A random pulsed load will be added to this to compare the performances obtained under variable load profile close to that of a real load.

The RES power profile (see first plot in Figure 14) is set using the PV, WT and random power profile, and associated gains (G_{PV}, G_{WT} and G_R). This high RES power profile that was set could appear during a sunny and windy day.

The FC response is shown in Figure 14 only for the Air-LF/Fuel-ESC control topology, but the results are almost the same for all control topologies. Note that the ESS power profile is the same with the RES power profile during the light or no load stages. The batteries stack is charged during these stages. Thus, an auxiliary load (electrolyzer, electrical vehicle or a dump load) must be connected if battery SOC increases above the upper limit. The FC will sustain the power flow during their specific load cycle of this auxiliary load if battery SOC falls below the lower limit.

The fuel efficiency indicator for all simulation diagrams under variable load and high RES power profile is shown in Figure 15. It can be noted that best values are also obtained for the Air-LF/Fuel-ESC and Air-sFF/Fuel-LF control topologies. For the Air-LF/Fuel-ESC control topology the fuel efficiency indicator is given also for 2 kW random RES profile. The shapes of the fuel efficiency indicators are almost the same and only a small difference appears in their values (see Figure 15, where both shapes are marked with ■).

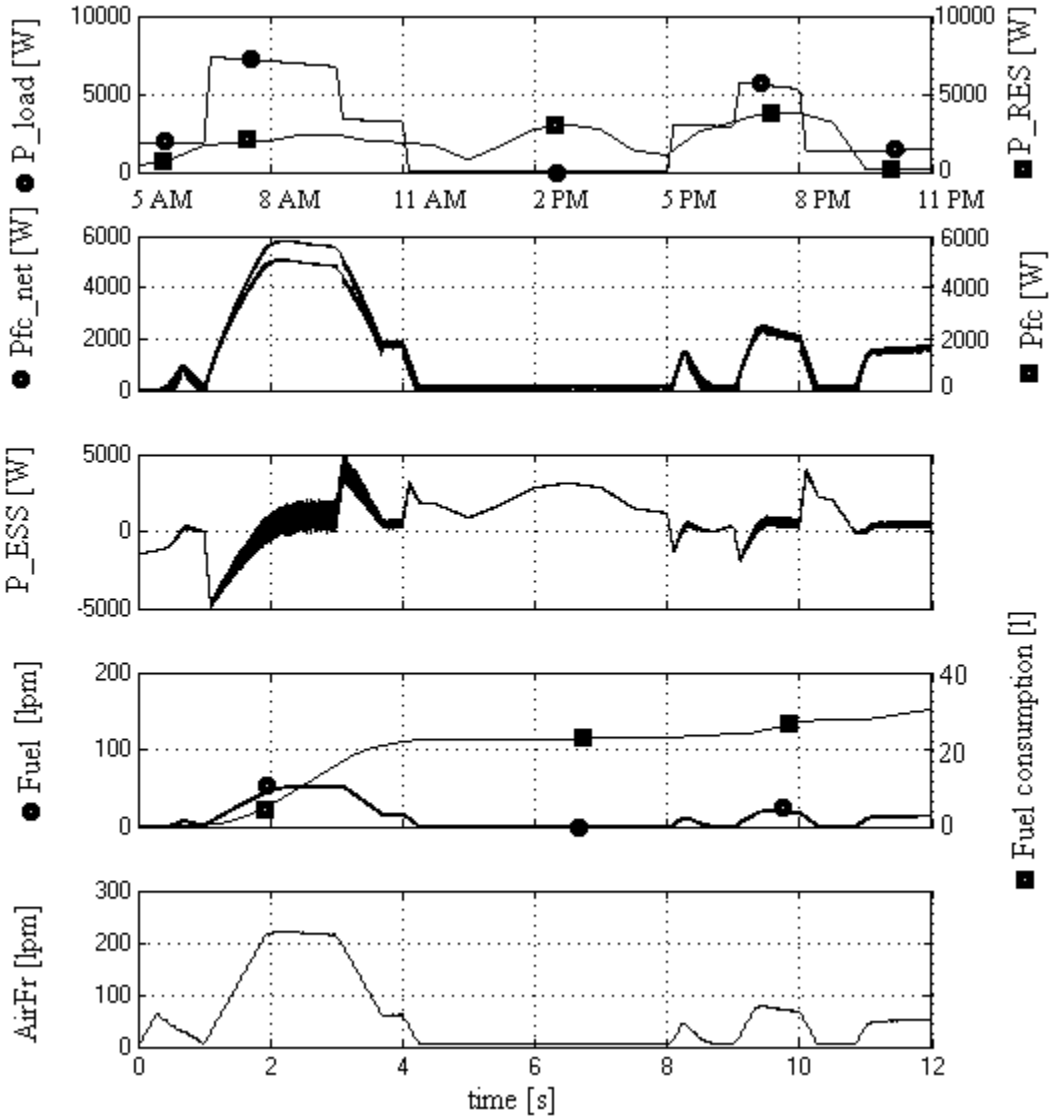

Figure 14. The FC response for Air-LF/ Fuel-ESC control topology under variable load and high RES power profile

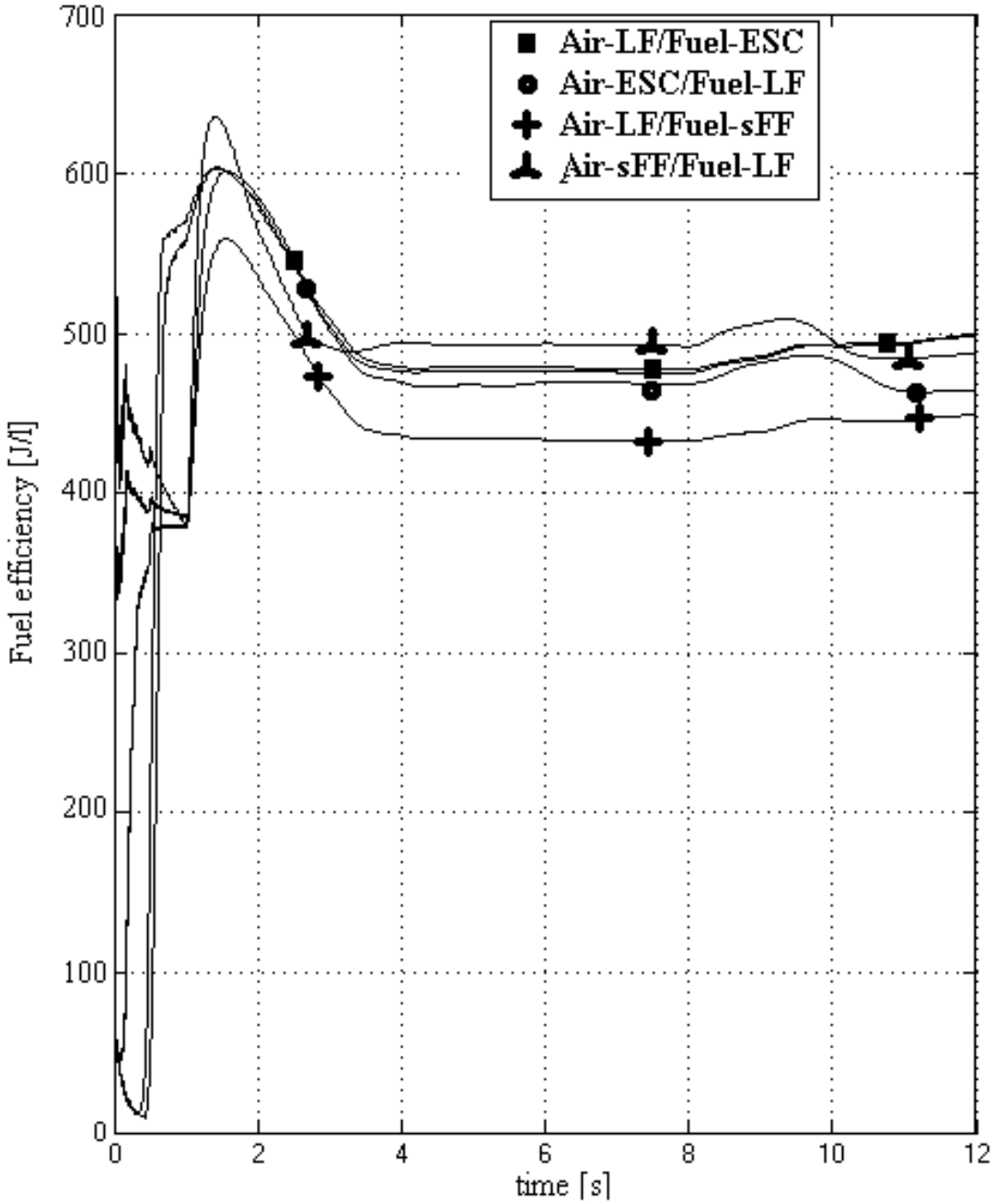

Figure 15. Fuel efficiency indicators for the simulation diagrams under variable load and high RES power profile

Two level of the random RES power profile are used in simulation (using as maximum/minimum limits the value of 1 kW and 2 kW, and sample times of 1 millisecond), but it was observed that the FC response is almost the same. Thus, only the results for 2 kW random RES power profile will be presented here. The random load profile is set using as maximum/minimum limits the value of 10 A (which means 250 W load power) and sample times of 0.5 second (to show how the FC net power tracks the pulsed load).

So, next step is to test the control topologies under the same load and RES power profiles, but with random power profile added as was defined above. 500 W and 2 kW random power profile is added to variable load and RES power profile.

A high RES power profile was set in Figure 16, which could appear during a sunny and windy day. The FC response is also shown in Figure 16 for the Air-LF/Fuel-ESC control topology. It can be observed that only the AV value of the needed power on the DC bus is generated by the FC system. The high frequency variations of

the power on the DC bus due to the random RES power or lack of power (at sharp and sudden changes in the load profile) are compensated by the ESS.
The fuel efficiency indicators for all simulation diagrams are shown in Figure 17. It can be noted that best values are also obtained for the Air-LF/Fuel-ESC and Air-sFF/Fuel-LF control topologies.

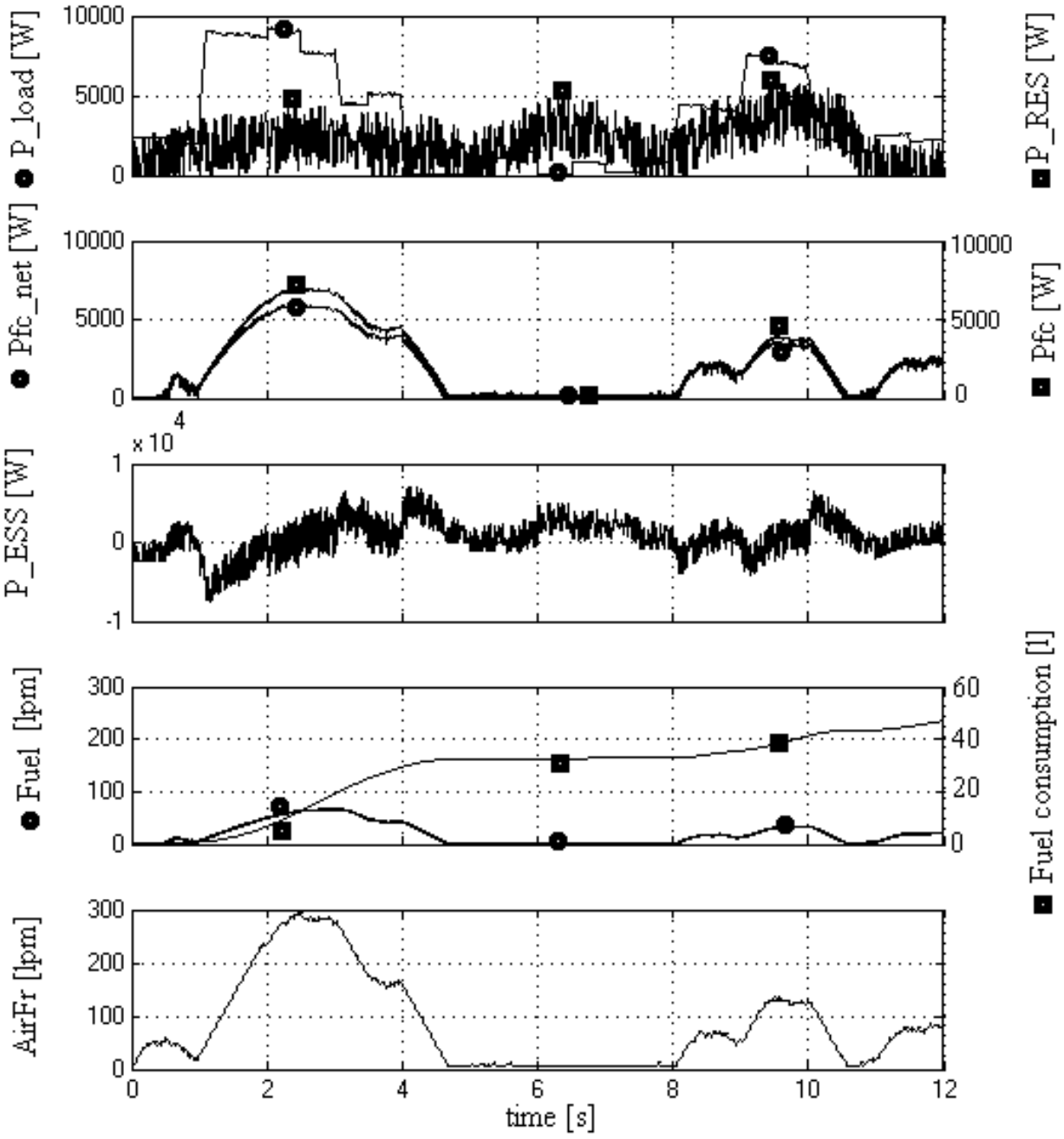

Figure 16. The FC response for Air-LF/ Fuel-ESC control topology under variable load and high RES power profile, having 500 W and 2 kW random power profile added

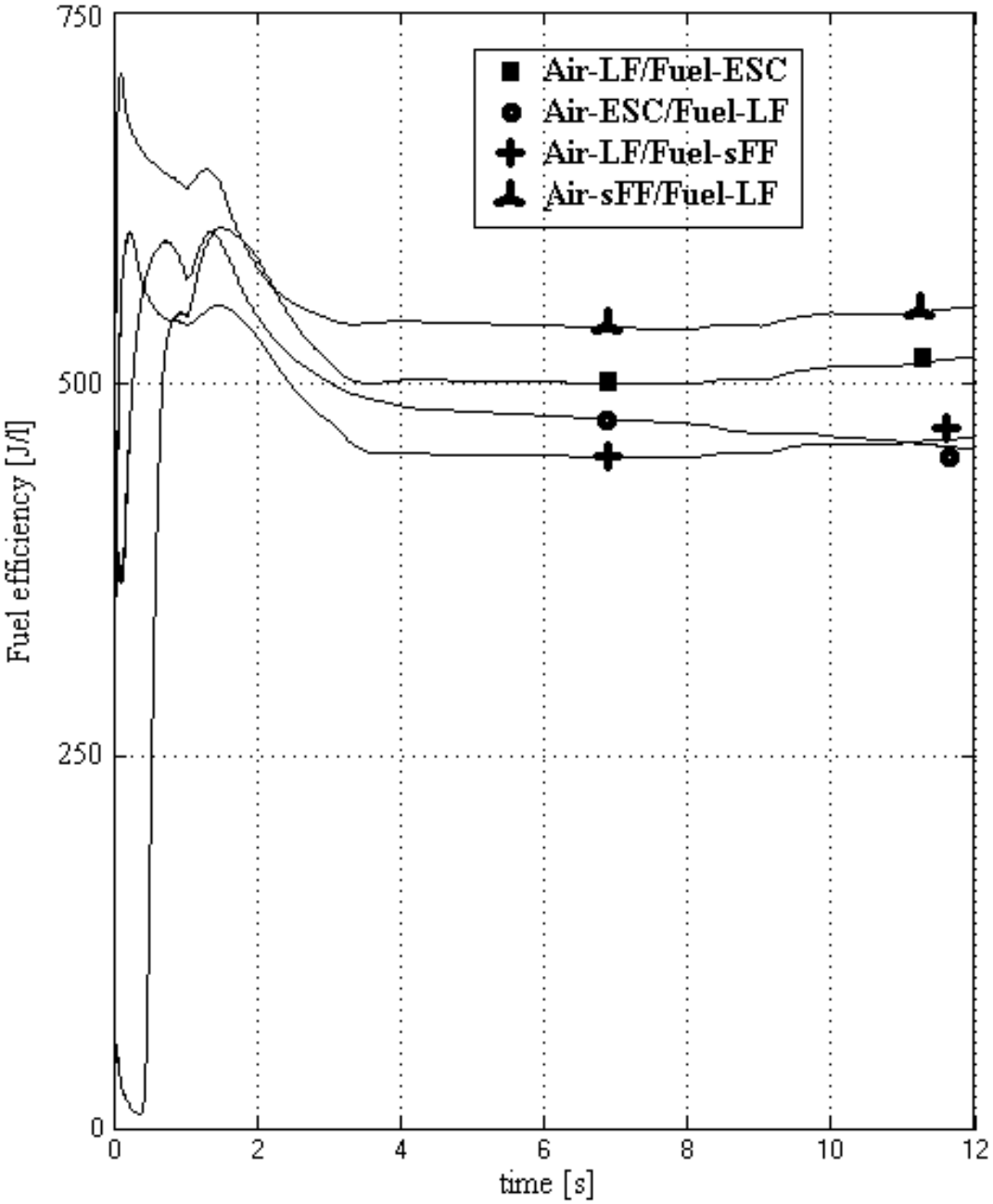

Figure 17. Fuel efficiency indicators for the simulation diagrams under variable load and high RES power profile, having 500 W and 2 kW random power profile added, respectively

The last step is to test the control topologies under the same load power profile, but under a low RES power profiles. The random load profile is set the same as above.

The low RES power profile (with 2 kW random power profile added) is shown in Figure 18. This is a RES power profile that could appear during a cloudy day with no wind. The FC response is also shown in Figure 18 for the Air-LF/Fuel-ESC control topology. It can be also observed that FC system operates in standby mode (at low power) during the light or no load stages. Thus, at 6 seconds, the FC system starts to generate power for a small and short pulse of the load that is over the AV RES power available. A circuit to detect these small and short pulses (for example, generated by fridge during night with no wind) will avoid such regimes for the FC system. Also, it can be noted that the AV value of the needed power on the DC bus is generated by the FC system and the high frequency variations of the power on the DC bus are compensated by the ESS. Note that the ESS operates in CS mode and the almost same ESS power profile is obtained in Figure 16 and 18.

The fuel efficiency indicators for low RES power profile are shown in Figure 19. The same order of control topologies analyzed is obtained.

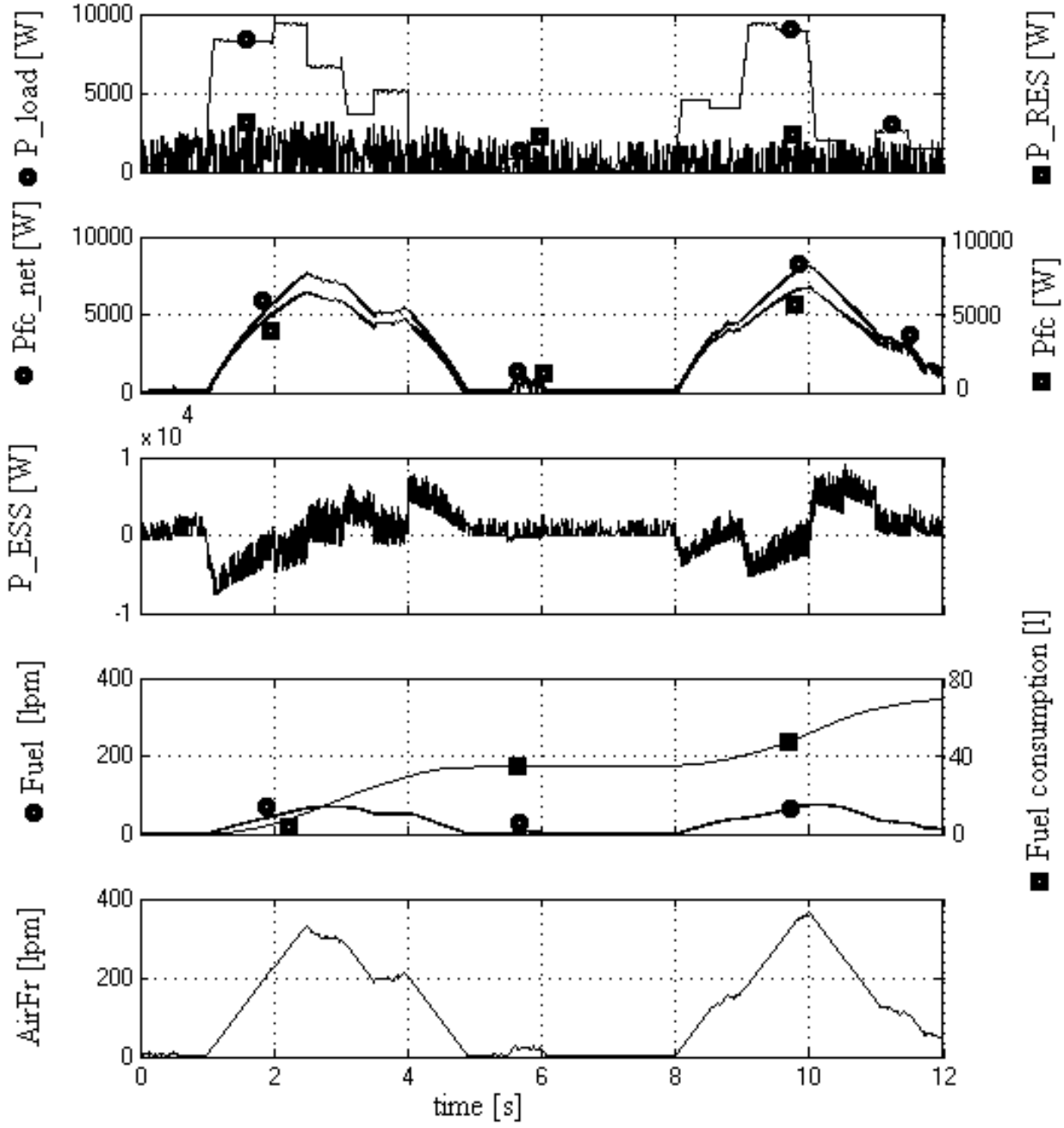

Figure 18. The FC response for Air-LF/ Fuel-ESC control topology under variable load and low RES power profile, having 500 W and 2 kW random power profile added, respectively

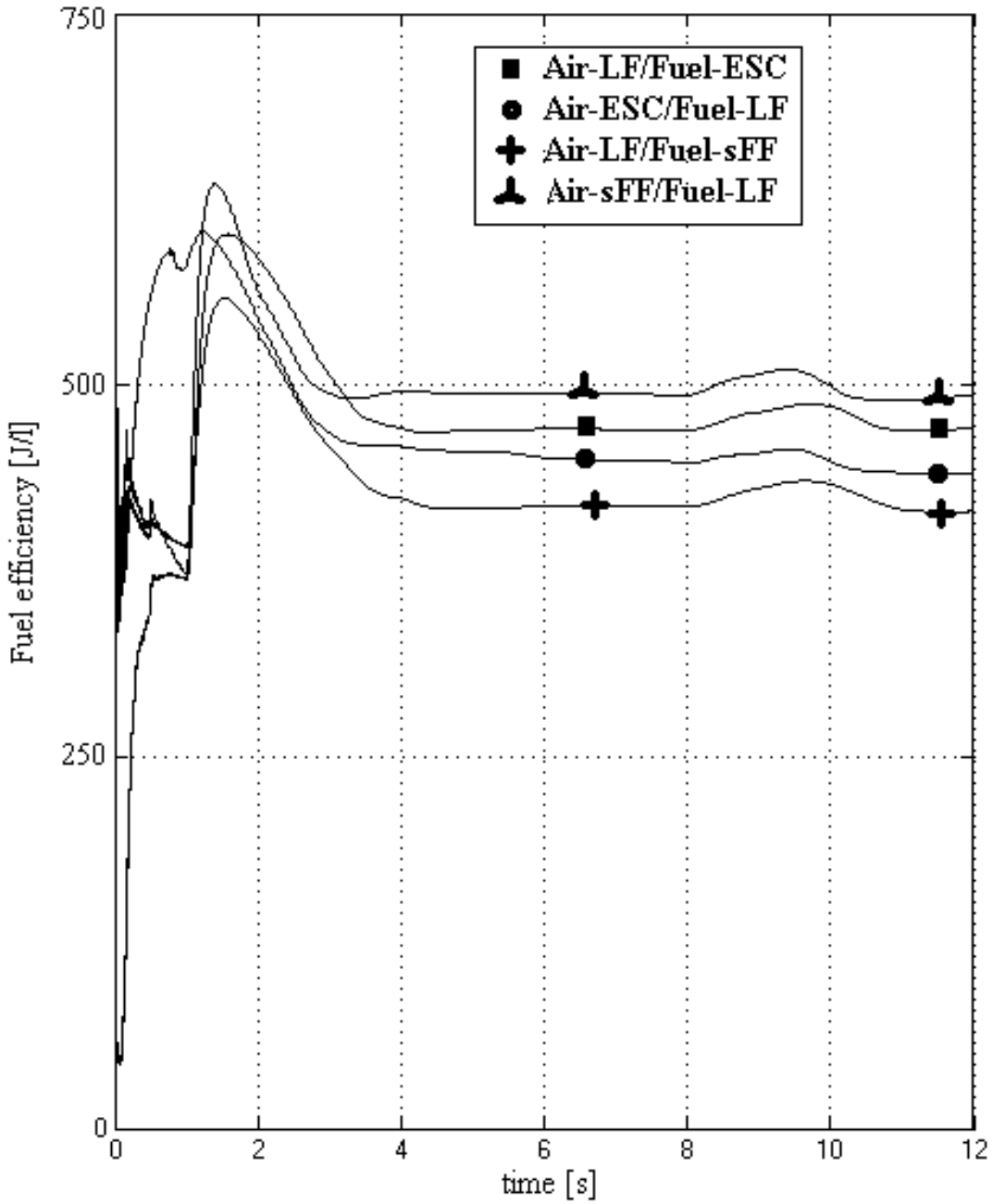

Figure 19. Fuel efficiency indicators for the simulation diagrams under variable load and low RES power profile, having 500 W and 2 kW random power profile added, respectively

The following remarks can be pointed out from the results shown in this section:
- The Air-LF/Fuel-ESC and Air-sFF/Fuel-LF control topologies are efficient for the FC HPS under pulsed loads (see Figure 13);
- The Air-LF/Fuel-ESC is recommended for the FC HPS under high load that operate the FC stack close to the FC rated power (see Figure 11);
- The Air-sFF/Fuel-LF control topology is efficient for the RES/FC HPS under different load and RES power profiles (see Figure 17 and 19);
- The Air-ESC/Fuel-LF control topology is efficient for the FC HPS used in FCV to minimize the fuel consumption (see Table 2);

Table 2. The reduction of the fuel consumption value for the Air-ESC/ Fuel-LF control diagram in comparison with the other control diagrams

I_{load} [A]	5	10	15	20	25	30
Fuel consumption for the Air-ESC/ Fuel-LF control diagram, F_{min} [l]	113.55	238.3	365	502.8	652.4	832.8
The minimum of the fuel consumption value for the other control diagrams, F_{other} [l]	127.5	273.3	419.3	587.2	720.4	838.1
Reduction of the fuel consumption, $(F_{other} - F_{min})/F_{min}$ [%]	12.29	30.82	47.82	74.33	59.89	4.67

These recommendations are also sustained by the results shown in the [37], where the FC system was directly loaded by a controlled current source. Note that the Air-ESC/Fuel-LF and Air-sFF/Fuel-LF control topologies were also compared in [36], but the FC system was directly loaded by a controlled current source.
The variability of the RES power profile is considered in performance evaluation of all control topologies analyzed here. The LF control loop for the FC net power is proposed to compensate the variability of the RES power profile. The control of the fuel in RES/FC HPS based on LF control seems to be the best EMU strategy under different load and RES power profiles.

7. Conclusion

Four control topologies applied to RES/FC HPS are analyzed in this paper under different load and RES power profiles. The variability of the RES power is the main issues in designing of the standalone RES/FC HPS to ensure safe and efficient operation of the FC system without use of a high ESS. Thus this is a challenging task for designing the EMU strategies and many proposals were made to predict the RES power flow and compensate the power flow balance on the DC bus from a backup energy source. The hybrid batteries/ultracapacitors ESS is usually used to compensate dynamically the power flow balance on the DC bus. Thus, a lot of EMU strategies were developed to control the power flows of FC, RES, batteries and/or ultracapacitors stacks in order to achieve the objectives mentioned above, including the economic aspects [65].
The LF control concept based on MEPT or sFF algorithm is proposed in this paper to sustain the load power demand under the daily variability of the RES power flow. Furthermore, the batteries stack will operate in CS mode if the LF control loop is implemented. Consequently, a small size of hybrid ESS is necessary to ensure the dynamic part of the power flow balance.
The main contributions of the analysis made in this paper are the following: (1) the Air-sFF/Fuel-LF control topology is more efficient that others control topologies analyzed under different load and RES power profiles (an increase of 3-5% of fuel efficiency indicator was observed in comparison with the Air-LF/Fuel-ESC control topology, which is the next control topology that ensure a high value of the fuel efficiency indicator); (2) the fuel consumption is minimum for the Air-ESC/Fuel-LF control topology (the reduction of the fuel consumption value for the Air-ESC/ Fuel-LF control diagram in comparison with the minimum value obtained with other control diagrams depends by the load, being in range of 5-75%); (3) both Air-LF/Fuel-ESC and Air-sFF/Fuel-LF control topologies are efficient for the FC HPS under pulsed loads; (4) the Air-LF/Fuel-ESC control topology is efficient at FC rated power (an increase of 6.7% of fuel efficiency indicator was observed in comparison with the Air-sFF/Fuel-LF control topology, which is the next control topology that ensure a high value of the fuel efficiency indicator). Consequently, the performances of the EMU strategy depend by the availability of the RES power, and level and dynamics of the load.

Acknowledgement. The research leading to these results has received funding from the Sectorial Operational Programme Human Resources Development (SOP HRD), financed from the European Social Fund and the Romanian Government under the contract number POSDRU /159 /1.5 /S/137390.

References

[1] Nikolova S, Causevski A, Al-Salaymeh A. Optimal operation of conventional power plants in power system with integrated renewable energy sources. Energy Convers Manage 2013;65: 697–703.
[2] Tascikaraoglu A, Boynuegri AR, Uzunoglu M. A Demand Side Management Strategy Based on Forecasting of Residential Renewable Sources: A Smart Home System in Turkey, Energ Buildings 2014;80:309-20.
[3] Tascikaraoglu A, Erdinc O, Uzunoglu M, Karakas A. An adaptive load dispatching and forecasting strategy for a virtual power plant including renewable energy conversion units. Appl Energ 2014;119:445-53.
[4] Ahmed NA, Miyatake M, Al-Othman AK. Power fluctuations suppression of stand-alone hybrid generation combining solar photovoltaic/wind turbine and fuel cell systems. Energy Convers Manage 2008;49:2711–19.
[5] García-Trivino P, et al. Long-term optimization based on PSO of a grid-connected renewable energy/battery/hydrogen hybrid system, Int J Hydrogen Energ 2014; 9(21):10805–16.
[6] Lior N. Sustainable energy development: The present (2009) situation and possible paths to the future, Energy 2010;35:3976–94.
[7] Carapellucci R, Giordano L. Modeling and optimization of an energy generation island based on renewable technologies and hydrogen storage systems. Int J Hydrogen Energy 2012;37(3):2081-93.
[8] Eroglu M, Dursun E, Sevencan S, Song J, Yazici S, Kilic O. A mobile renewable house using PV/wind/fuel cell hybrid power system. Int J Hydrogen Energy 2011;36(13):7985-92.
[9] Erdinc O, Uzunoglu M. A new perspective in optimum sizing of hybrid renewable energy systems: consideration of component performance degradation issue. Int J Hydrogen Energy 2012;37(14):10479-88.
[10] Onur E, Ugur SS. A comparative sizing analysis of a renewable energy supplied stand-alone house considering both demand side and source side dynamics. Appl Energ 2012;96:400-8
[11] Hannan MA, Azidin FA, Mohamed A. Multi-sources model and control algorithm of an energy management system for light electric vehicles. Energy Convers Manage 2012;62:123–30.
[12] Castaneda M, Cano A, Jurado F, Sanchez H, Fernandez LM. Sizing optimization, dynamic modeling and energy management strategies of a stand-alone PV/hydrogen/battery-based hybrid system. Int J Hydrogen Energy 2013;38(10):3830-45.
[13] Trifkovic M, Sheikhzadeh M, Nigim K, Daoutidis P. Modeling and control of a renewable hybrid Energy system with hydrogen storage. IEEE Trans Control Syst Technol 2014;22(1):169-79.
[14] Bajpai P, Dash V. Hybrid renewable energy systems for power generation in stand-alone applications: a review. Renew Sustain Energy Rev 2012;16(5):2926-39.
[15] Bizon N. Load-following Mode Control of a Standalone Renewable/Fuel Cell Hybrid Power Source, Energy Convers Manage 2014;77:763–72.
[16] Auld AE, Smedley KM, Mueller F, Brouwer J, Samuelsen GS. Load-following active power filter for a solid oxide fuel cell supported load. J Power Sources 2010;195(7): 1905-13.
[17] Smith AD, Mago PJ. Effects of load-following operational methods on combined heat and power system efficiency. Appl Energ 2014;115:337-51.
[18] Etxeberria A, Vechiu I, Camblong H, Vinassa J-M. Comparison of three topologies and controls of a hybrid energy storage system for microgrids. Energy Convers Manage 2012;54:113–21.
[19] Feroldi D, Zumoffen D. Sizing methodology for hybrid systems based on multiple renewable power sources integrated to the energy management. Int J Hydrogen Energy 2014;39:8609-20.
[20] Chen P-C. Robust voltage tracking control for proton exchange membrane fuel cells. Energy Convers Manage 2013;65:408–19.
[21] Torreglosa JP, García P, Fern_andez LM, Jurado F. Hierarchical energy management system for stand-alone hybrid system based on generation costs and cascade control. Energy Convers Manage 2014;77:514-26.
[22] Caisheng W, Nehrir MH. Power management of a standalone wind/photovoltaic/fuel cell energy system. IEEE Trans Energy Convers 2008;23(3):957-67
[23] Erdinc O, Uzunoglu M. The importance of detailed data utilization on the performance evaluation of a grid independent hybrid renewable energy system. Int J Hydrogen Energy 2011;36(20):12664-77.
[24] Erdinc O, Elma O, Uzunoglu M, Selamogullari US, Vural B, Ugur E, et al. Experimental performance assessment of an online energy management strategy for varying renewable power production suppression. Int J Hydrogen Energy 2012;37(6):4737-48.

[25] Thounthong P, Chunkag V, Sethakul P, Sikkabut S, Pierfederici S, Davat B. Energy management of fuel cell/solar cell/supercapacitor hybrid power source. J Power Sources 2011;196(1):313-24.
[26] Nikolova S, Causevski A, Al-Salaymeh A. Optimal operation of conventional power plants in power system with integrated renewable energy sources. Energy Convers Manage 2013;65:697–703.
[27] Bizon N, Tabatabaei NM, Shayeghi H. Analysis, Control and Optimal Operations in Hybrid Power Systems, Advanced Techniques and Applications for Linear and Nonlinear Systems, London: Springer Verlang; 2013
(available at http://www.springer.com/engineering/control/book/978-1-4471-5537-9)
[28] Garcia P, Garcia CA, Fernandez LM, Llorens F, Jurado F. ANFIS-based control of a grid-connected hybrid system integrating renewable energies, hydrogen and batteries. IEEE Trans Indus Inform 2014;10(2):1107-17.
[29] El-Shatter TF, Eskander MN, El-Hagry MT. Energy flow and management of a hybrid wind/PV/fuel cell generation system. Energy Convers Manage 2006;47(9–10):1264-1280.
[30] Trifkovic M, Sheikhzadeh M, Nigim K, Daoutidis P. Modeling and control of a renewable hybrid Energy system with hydrogen storage. IEEE Trans Control Syst Technol 2014;22(1):169-79.
[31] Gillenwater M. Probabilistic decision model of wind power investment and influence of green power market. Energ Policy 2013;63:1111–25.
[32] Giannakoudis G, Papadopoulos AI, Seferlis P, Voutetakis S. Optimum design and operation under uncertainty of power systems using renewable energy sources and hydrogen storage. Int J Hydrogen Energy 2009;35:872-91.
[33] Xu, L., Li, J., Ouyang, M., Hua, J., Yang, G. Multi-mode control strategy for fuel cell electric vehicles regarding fuel economy and durability. Int J Hydrogen Energy 2014;39(5):2374–2389.
[34] Chiniforoosh S, et all. Definitions and Applications of Dynamic Average Models for Analysis of Power Systems. IEEE T Power Deliver 2010;25(4):2655-69.
[35] Bizon N. Energy harvesting from the FC stack that operates using the MPP tracking based on modified extremum seeking control. Appl Energ 2013;104:326-36.
[36] Bizon N. Tracking the maximum efficiency point for the FC system based on extremum seeking scheme to control the air flow. Appl Energ 2014;129:147–57.
[37] Bizon N. Improving the PEMFC energy efficiency by optimizing the fuelling rates based on extremum seeking algorithm. Int J Hydrogen Energy 2014;39(20):10641–54.
[38] Bajpai P, Dash V. Hybrid renewable energy systems for power generation in stand-alone applications: A review. Renew Sust Energ Rev 2012;16:2926–39.
[39] Restrepo C, Ramos-Paja CA, Giral R, Calvente J, Romero A. Fuel cell emulator for oxygen excess ratio estimation on power electronics applications, Comp Elec Eng 2012; 38:926–37.
[40] Bizon N. Advances in Energy Research: Distributed Generation systems integrating Renewable Energy Resources, Nova Science Publishers Inc., NY: 2012
(available at https://www.novapublishers.com/catalog/product_info.php?products_id=22516)
[40] Farret FA, Simões MG. Integration of Alternative Sources of Energy, Hoboken, NJ: Wiley; 2006.
[41] Chauhan A, Saini RP. A review on Integrated Renewable Energy System based power generation for stand-alone applications: Configurations, storage options, sizing methodologies and control. Renew Sust Energ Rev 2014;38:99–120.
[42] Markvart T, Castaner L. Practical handbook of photovoltaics: fundamentals and applications. Elsevier; 2003.
[43] Agustin JLB, Lopez RD. Simulation and optimization of stand-alone hybrid renewable energy systems. Renew Sust Energ Rev 2009;13(8):2111–8.
[44] Li C-H, Zhu X-J, Cao G-Y, Sui S, Hu M-R. Dynamic modeling and sizing optimization of stand-alone photovoltaic power systems using hybrid energy storage technology. Renew Energ 2009;32(3):815–26.
[45] Erdinc O, Vural B, Uzunoglu M. A wavelet-fuzzy logic based energy management strategy for a fuel cell/battery/ultra-capacitor hybrid vehicular power system. J Power Sources 2009;194:369-80.
[46] Thounthong P, Tricoli P, Davat B. Performance investigation of linear and nonlinear controls for a fuel cell/supercapacitor hybrid power plant. Int Journal Elec Power 2014;54:454–64.
[47] Jacobus H, Lin B, Jimmy DH, Ansumana R, Malanoski AP, Stenger D. Evaluating the impact of adding energy storage on the performance of a hybrid power system. Energy Convers Manage 52 (2011) 2604–2610.

[48] Ramos-Paja CA, Spagnuolo G, Petrone G, Mamarelis E. A perturbation strategy for fuel consumption minimization in polymer electrolyte membrane fuel cells: Analysis, Design and FPGA implementation. Appl Energ 2014;119:21–32.
[49] Payman A, Pierfederici S, Meibody-Tabar F. Energy control of supercapacitor/fuel cell hybrid power source. Energy Convers Manage 2008;49:1637–1644.
[50] Peng FZ, Yuvan X, Fang X, Qian Z. Z-source inverter for motor drives. IEEE Trans Power Electron 2005;20(4): 857-63.
[51] De Bernardinis A. Synthesis on power electronics for large fuel cells: From power conditioning to potentiodynamic analysis technique. Energy Convers Manage 2014;84:174–85.
[52] Pei P, Chen H. Main factors affecting the lifetime of Proton Exchange Membrane fuel cells in vehicle applications: A review. Appl Energ 2014;125:60–75.
[53] Corbo P, Migliardini F, Veneri O, Experimental analysis and management issues of a hydrogen fuel cell system for stationary and mobile application, Energy Convers Manage 2007;48 (8):2365-2374.
[54] Feroldi D, Serra M, Riera J. Energy Management Strategies based on efficiency map for Fuel Cell Hybrid Vehicles. J Pow Sour 2009;190: 387–401.
[55] Ipsakisa D, Voutetakisa S, Seferlisa P, Stergiopoulos F, Elmasides C. Power management strategies for a stand-alone power system using renewable energy sources and hydrogen storage. Int J Hydrogen Energy 2010;34:7081–95.
[56] Bruni G, Cordiner S, V. Mulone V. Domestic distributed power generation: Effect of sizing and energy management strategy on the environmental efficiency of a photovoltaic-battery-fuel cell system, Energy 2014, http://dx.doi.org/10.1016/j.energy.2014.05.062
[57] SimPowerSystems TM Reference, Hydro-Québec and the MathWorks, Inc., Natick, MA; 2010.
[58] Becherif M, Hissel D. MPPT of a PEMFC based on air supply control of the motocompressor group. Int J Hydrogen Energ 2010; 35(22): 12521–30.
[59] Gou B, Na WK, Diong B. Fuel Cells: Modeling, Control, and Applications, CRC Press 2010: 6.
[60] Pukrushpan JT, Stefanopoulou AG, Peng H. Control of fuel cell power systems: principles, modeling, analysis, and feedback design. London: Springer Verlag; 2004.
[61] Majidpour M, Chen WP. Grid and Schedule Constrained Electric Vehicle Charging Algorithm Using Node Sensitivity Approach, ICCVE 2012:304-10.
[62] Nelms RM, Spyker RL. Classical equivalent circuit parameters for a double-layer capacitor. IEEE Trans Aerosp Electron Syst 2000;36(3):829–36.
[63] Weidner JW, Srinivasan V. Mathematical modeling of electrochemical capacitors. J Electrochem Soc 1999;146(5):1650–8.
[64] Bizon N. Energy efficiency of multiport power converters used in plug-in/V2G fuel cell vehicles. Appl Energ 2012;96: 431–443.
[65] Yohanis Y, Mondol J, Wright A, Norton B. Real-life energy use in the UK: How occupancy and dwelling characteristics affect domestic electricity use. Energ Buildings 2008;40:1053–59.
[66] Kunusch C, Puleston PF, Mayosky MA, Riera J. Sliding mode strategy for PEM fuel cells stacks breathing control using a super–twisting algorithm. IEEE T Contr Syst T 2009;17(1): 167–73.
[67] Erdinc O. Economic Impacts of Small-Scale Own Generating and Storage Facilities, and Electric Vehicles under Different Demand Response Strategies for Smart Households. Appl Energ 2014;126:142-50.